



# Studies Of Various Parameters Of Micro Strip Filter Using Various Software's

Author: Malay Karmakar Senior Research Assistant at IIT Kharagpur (ECE Dept.)

## Abstract:-

A micro strip filter is an electronic filter that uses micro strip transmission lines to create circuitry that selectively leaves or blocks certain frequency signals. It is a passive device commonly used in communications, radar, and other electronic systems to reduce unwanted signals or noise and improve the quality of desired signals. The filter works by combining the effects of distributed capacitance, inductance and resistance in the micro strip transmission line and the placement of resonators such as capacitors or coils to create bandpass, low pass or high pass. Micro strip filters can be designed with narrow or wide bandwidth, high or low insertion loss, and high or low attenuation. They are compact and lightweight, allowing easy integration into printed circuit boards (PCBs) or other circuits. By applying a high frequency microwave signal, its h-parameter, s-parameter, y-parameter, z-parameter and Smith diagram are investigated. For this, we used 3 software HFSS, CST and IE3D. The results are consistent with almost any software.

## CHAPTER -1

**INTRODUCTION:** Micro strip Phase Bridge/Filters play important roles in many RF/microwave applications. Emerging applications such as wireless communications continue to challenge RF/microwave filters with ever more stringent requirements – higher performance, smaller size, lighter weight, and lower cost. The recent advances in novel materials and fabrication technologies, including high-temperature superconductors (HTS), low-temperature co fired ceramics (LTCC), monolithic microwave integrated circuits (MMIC), microelectromechanical system (MEMS), and micromachining technology, have stimulated the rapid development of new micro strip and other filters for RF/microwave applications. In the meantime, advances in computer-aided design (CAD) tools such as full-wave electromagnetic (EM) simulators have revolutionized filter design. Many novel micro strip filters with advanced filtering characteristics have been demonstrated. However, up until now there has not been a single book dedicated to this subject.

*Micro strip Filters for RF/Microwave Applications*<sup>[1]</sup> offers a unique and comprehensive treatment of RF/microwave filters based on the micro strip structure, providing a link to applications of computer-aided design tools and advanced materials and technologies. Many novel and sophisticated filters using computer-aided design are discussed, from basic concepts to practical realizations.

The outstanding features of this filter include discussion of many novel micro strip configurations with advanced filtering characteristics, new design techniques, and methods for filter miniaturization. It emphasizes computer analysis and synthesis and full-wave electromagnetic (EM) simulation through a large number of design examples. Applications of commercially available software are demonstrated. Commercial applications are included as are design theories and methodologies, which are not only for micro strip filters, but also directly applicable to other types of filters, such as waveguide and other transmission line filters. Therefore, this book is more than just a text on micro strip filters.

Much of work described herein has resulted from the authors' research. The authors wish to acknowledge the financial support of the UK EPSRC and the European Commission through the Advanced Communications Technologies and Services (ACTS) program. They would also like to acknowledge their national and international collaborators, including Professor Heinz Chaloupka at Wuppertal University (Germany), Robert Greed at Marconi Research Center (U.K.), Dr. Jean-Claude Mage at Thomson-CSF/CNRS (France), and Dieter Jedamzik, formerly with GEC-Marconi Materials Technology (U.K.).

The authors are indebted to many researchers for their published works, which were rich sources of reference. Their sincere gratitude extends to the Editor of the Wiley Series in Microwave and Optical Engineering, Professor Kai Chang; the Executive Editor of Wiley-Interscience, George Telecki; and the reviewers for their support in writing the book. The help provided by Cassie Craig and other members of the staff at Wiley is most appreciated. The authors also wish to thank their colleagues at the University of Birmingham, including Professor Peter Hall, Dr. Fred Huang, Dr. Adrian Porch, and Dr. Peter Gardener.

In addition, Jia-Sheng Hong would like to thank Professor John Allen at the University of Oxford (U.K.), Professor Werner Wiesbeck at Karlsruhe University (Germany), and Dr. Nicholas Edwards at British Telecom (U.K.) for their many years of support and friendship. Professor Joseph Helszain at Heriot-Watt University (U.K.), who sent his own book on filters to Jia-Sheng Hong, is also acknowledged.

Finally, Jia-Sheng Hong would like to express his deep appreciation to his wife, Kai, and his son, Haide, for their tolerance and support, which allowed him to write the book at home

over many evenings, weekends, and holidays. In particular, without the help of Kai, completing this book on time would not have been possible.

## CHAPTER -2

### MICRO STRIP FILTER

First of all Micro strip Phase Bridge is a Filter which can be realized in two ways

- 1) By using LC (lumped) Component Approach.
- 2) By using Distributed Transmission Line Approach.

LC lumped Component cannot be used as a Filter at high frequencies because as frequency increases there is a reduction in wavelength. So, we have to go through a Distributed Approach. In Distributed Approach we can use Micro strip Filter which is used in Transmission Line.

Micro strip Line is one of the most popular types of Planar transmission Line, primarily because it can be fabricated by Photolithographic Process and is easily integrated with other passive and active microwave devices. The geometry of a Micro strip Line is shown below.

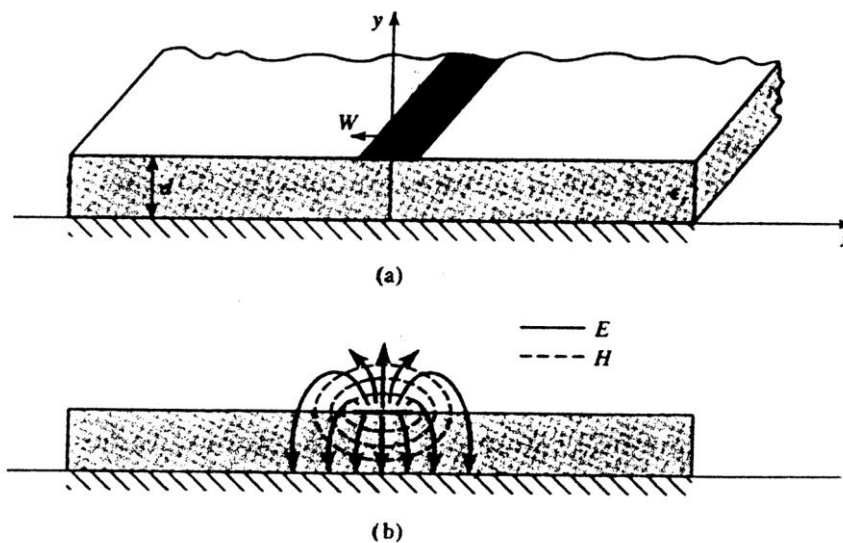


Fig. 2.1 Micro strip transmission line. (a) Geometry. (b) Electric & magnetic field lines.

### 2.1 Micro strip

Micro strip line is one of the most popular types of planar transmission lines, primarily because it can be fabricated by photolithographic processes and is easily integrated with other passive and active microwave devices. The geometry of a micro strip line is shown in Figure 2.1 (a). A conductor of width  $W$  is printed on a thin, grounded dielectric substrate of thickness  $d$  and relative permittivity  $\epsilon_r$ ; a sketch of the field lines is shown in Figure 2.1 (b).

If the dielectric were not present ( $\epsilon_r = 1$ ), we could think of the line as a two-wire line consisting of two flat strip conductors of width  $W$ , separated by a distance  $2d$  (the ground plane

can be removed via image theory). In this case we would have a simple TEM transmission line, with  $v_p = c$  and  $\beta = k_0$ .

The presence of the dielectric, and particularly the fact that the dielectric does not fill the air region above the strip ( $y > d$ ), complicates the behavior and analysis of the micro strip line. Unlike strip line, where all the fields are contained within a homogeneous dielectric region, micro strip has some (usually most) of its field lines in the dielectric region, concentrated between the strip conductor and the ground plane, and some fraction in the air region above the substrate. For this reason the micro strip line cannot support a pure TEM wave, since the phase velocity of TEM fields in the dielectric region would be  $c/\sqrt{\epsilon_r}$ , but the phase velocity of TEM fields in the air region would be  $c$ . Thus a phase match at the dielectric air interface would be impossible to attain for a TEM-type wave.

In actually, the exact fields of a micro strip line constitute a hybrid TM-TE wave, and require more advanced analysis techniques than we are prepared to deal with here. In most practical applications, however, the dielectric substrate is electrically very thin ( $d \ll \lambda$ ), and so the fields are quasi-TEM. In other words, the fields are essentially the same as those of the static case. Thus, good approximations for the phase velocity, propagation constant and characteristic impedance can be obtained from static or quasi-static solutions. Then the phase velocity propagation constant can be expressed as

$$v_p = \frac{c}{\sqrt{\epsilon_e}} \quad \dots 2.1$$

$$\beta = k_0 \frac{c}{\sqrt{\epsilon_e}} \quad \dots 2.2$$

where  $\epsilon_e$  is the effective dielectric constant of the micro strip line. Since some of the field lines are in the dielectric region and some are in air, the effective dielectric constant satisfies the relation

$$1 < \epsilon_e < \epsilon_r$$

and is dependent on the substrate thickness,  $d$ , and conductor width,  $W$ .

We will first present design formulas for the effective dielectric constant and characteristic impedance of micro strip line; these results are curve-fit approximations to rigorous quasi-static solutions [8], [9]. Then we will outline a numerical method of solution (similar to that used in the previous section for strip line) for the capacitance per unit length of micro strip line.

## 2.2 Formulas for Effective Dielectric Constant, Characteristic Impedance, and Attenuation

The effective dielectric constant of a micro strip line is given approximately by

$$\epsilon_e = \frac{\epsilon_r + 1}{2} + \frac{\epsilon_r - 1}{2} \frac{1}{\sqrt{1 + 12d/W}} \quad \dots 2.3$$

The effective dielectric constant can be interpreted as the dielectric constant of a homogeneous medium that replaces the air and dielectric regions of the micro strip, as shown in Figure 2.2. The phase velocity and propagation constant are then given by equations 2.1 and 2.2.

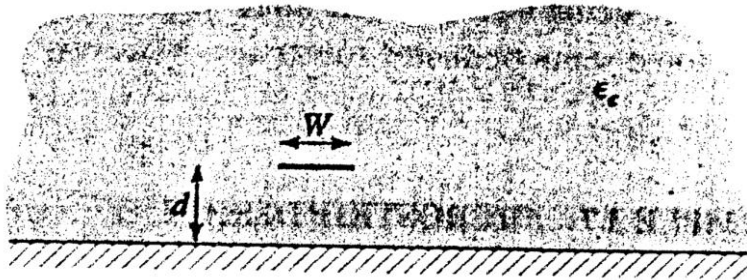


Fig. 2.2 Equivalent geometry of quasi-TEM micro strip line, where the dielectric slab of thickness  $d$  and relative permittivity  $\epsilon_r$  has been replaced with homogenous medium of effective relative permittivity,  $\epsilon_e$

Given the dimensions of the micro strip line, the characteristic impedance can be calculated as

$$Z_0 = \begin{cases} \frac{60}{\sqrt{\epsilon_e}} \ln \left( \frac{8d}{W} + \frac{W}{4d} \right) & \text{for } W/d \leq 1 \\ \frac{120\pi}{\sqrt{\epsilon_e} \left[ W/d + 1.393 + 0.667 \ln(W/d + 1.444) \right]} & \text{for } W/d \geq 1 \end{cases} \quad \dots 2.4$$

For a given characteristic impedance  $Z_0$  and dielectric constant  $\epsilon_r$ ,  $W/d$  ratio can be found as

$$\frac{W}{d} = \begin{cases} \frac{8e^A}{e^{2A} - 2} & \text{for } W/d < 2 \\ \frac{2}{\pi} \left[ B - 1 - \ln(2B - 1) + \frac{\epsilon_r - 1}{2\epsilon_r} \left\{ \ln(B - 1) + 0.39 - \frac{0.61}{\epsilon_r} \right\} \right] & \text{for } W/d > 2 \end{cases} \quad \dots 2.5$$

Where

$$A = \frac{Z_0}{60} \sqrt{\frac{\epsilon_r + 1}{2}} + \frac{\epsilon_r - 1}{\epsilon_r + 1} \left( 0.23 + \frac{0.11}{\epsilon_r} \right)$$

$$B = \frac{377\pi}{2Z_0\sqrt{\epsilon_r}}$$



Considering micro strip as a quasi-TEM line, the attenuation due to dielectric loss can be determined as

$$\alpha_d = \frac{k_0 \epsilon_r (\epsilon_e - 1) \tan \delta}{2 \sqrt{\epsilon_e} (\epsilon_r - 1)} Np / m, \quad \dots 2.6$$

where  $\tan \delta$  is the loss tangent of the dielectric. This result is derived from  $\alpha_d = \frac{k \tan \delta}{2} Np / m$  by multiplying by a “filling factor”.

$$\frac{\epsilon_r (\epsilon_e - 1)}{\epsilon_e (\epsilon_r - 1)}$$

which accounts for the fact that the fields around the micro strip line are partly in air (lossless) and partly in the dielectric. The attenuation due to conductor loss is given approximately by

$$\alpha_c = \frac{R_s}{Z_0 W} Np / m, \quad \dots 2.7$$

where  $R_s = \sqrt{\omega \mu_0 / 2 \sigma}$  is the surface resistivity of the conductor. For most micro strip substrates, conductor loss is much more significant than dielectric loss; exceptions may occur with some semiconductor substrates, however.

### 2.3 An Approximate Electrostatic Solution

We now look at an approximate quasi-static solution for the micro strip line, so that the appearance of design equations like those of eqn. 2.3-2.5 is not a complete mystery. This analysis is very similar to that carried out for strip line in the previous section. As in that analysis, it is again convenient to place conducting sidewalls on the micro strip line, as shown in Figure 2.3. The sidewalls are placed at  $x = \pm a/2$ , where  $a \gg d$ , so that the walls should not perturb the field lines localized around the strip conductor. We then can solve Laplace's equation in the region between the sidewalls :

$$\nabla^2 \Phi(x, y) = 0, \quad \text{for } |x| \leq a/2, 0 \leq y < \infty \quad \dots 2.8$$

with boundary conditions,

$$\begin{aligned} \Phi(x, y) &= 0 \quad \text{at } x = \pm a/2 \\ \Phi(x, y) &= 0 \quad \text{at } y = 0, \infty \end{aligned} \quad \dots 2.9 \text{ a, b}$$

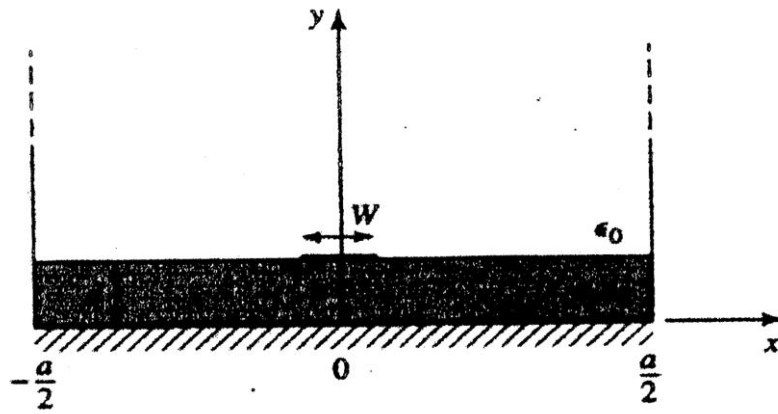


Fig. 2.3 Geometry of a microstrip line with conduction sidewalls

Since there are two regions defined by the air/dielectric interface, with a charge discontinuity on the strip, we will have separate expressions for  $\Phi(x,y)$  in these regions. Solving (2.8) by the method of separation of variables and applying the boundary conditions of (2.9 a, b) gives the general condition as

$$\Phi(x,y) = \begin{cases} \sum_{\substack{n=1 \\ \text{odd}}}^{\infty} A_n \cos \frac{n\pi x}{a} \sinh \frac{n\pi y}{a} & \text{for } 0 \leq y \leq d \\ \sum_{\substack{n=1 \\ \text{odd}}}^{\infty} B_n \cos \frac{n\pi x}{a} e^{-n\pi y/a} & \text{for } d \leq y \leq \infty \end{cases} \quad \dots 2.10$$

Now the potential must be continuous at  $y = d$ , so from (2.10) we have that

$$A_n \sinh \frac{n\pi d}{a} = B_n e^{-n\pi d/a} \quad \dots 2.11$$

so  $\Phi(x,y)$  can be written as

$$\Phi(x,y) = \begin{cases} \sum_{\substack{n=1 \\ \text{odd}}}^{\infty} A_n \cos \frac{n\pi x}{a} \sinh \frac{n\pi y}{a} & \text{for } 0 \leq y \leq d \\ \sum_{\substack{n=1 \\ \text{odd}}}^{\infty} A_n \cos \frac{n\pi x}{a} \sinh \frac{n\pi d}{a} e^{-n\pi(y-d)/a} & \text{for } d \leq y \leq \infty \end{cases} \quad \dots 2.12$$

The remaining constants,  $A_n$  can be found by considering the surface charge density on the strip. We first find  $E_y = -\partial\Phi / \partial y$ :

$$E_y = \begin{cases} -\sum_{\substack{n=1 \\ \text{odd}}}^{\infty} A_n \left(\frac{n\pi}{a}\right) \cos \frac{n\pi x}{a} \cosh \frac{n\pi y}{a} & \text{for } 0 \leq y \leq d \\ \sum_{\substack{n=1 \\ \text{odd}}}^{\infty} A_n \left(\frac{n\pi}{a}\right) \cos \frac{n\pi x}{a} \sinh \frac{n\pi d}{a} e^{-n\pi(y-d)/a} & \text{for } d \leq y \leq \infty \end{cases} \quad \dots 2.13$$

Then the surface charge density on the strip at  $y=d$  is

$$\begin{aligned}
\rho_s &= D_y(x, y=d^+) - D_y(x, y=d^-) \\
&= \epsilon_0 E_y(x, y=d^+) - \epsilon_0 \epsilon_r E_y(x, y=d^-) \quad \dots 2.14 \\
&= \epsilon_0 \sum_{\substack{n=1 \\ \text{odd}}}^{\infty} A_n \left( \frac{n\pi}{a} \right) \cos \frac{n\pi x}{a} \left[ \sinh \frac{n\pi d}{a} + \epsilon_r \cosh \frac{n\pi d}{a} \right]
\end{aligned}$$

Which is seen to be a Fourier series in x for the surface charge density,  $\rho_s$ . As for the strip line case, we can approximate the charge density on the micro strip line by a uniform distribution:

$$\rho_s(x) = \begin{cases} 1 & \text{for } |x| < W/2 \\ 0 & \text{for } |x| > W/2 \end{cases} \quad \dots 2.15$$

Equation (2.15) to (2.14) and using the orthogonality of the  $\cos n\pi x/a$  functions gives the constants  $A_n$  as

$$A_n = \frac{4a \sin n\pi W/2a}{(n\pi)^2 \epsilon_0 \left[ \sinh(n\pi d/a) + \epsilon_r \cosh(n\pi d/a) \right]} \quad \dots 2.16$$

The voltage of the strip relative to the ground plane is

$$V = - \int_0^d E_y(x=0, y) dy = \sum_{\substack{n=1 \\ \text{odd}}}^{\infty} A_n \sinh \frac{n\pi d}{a} \quad \dots 2.17$$

The total charge, per unit length, on the Centre strip is

$$Q = \int_{-W/2}^{W/2} \rho_s(x) dx = WC/m, \quad \dots 2.18$$

so the static capacitance per unit length of the micro strip line is

$$C = \frac{Q}{V} = \frac{1}{\sum_{\substack{n=1 \\ \text{odd}}}^{\infty} \frac{4a \sin(n\pi W/2a) \sinh(n\pi d/a)}{(n\pi)^2 W \epsilon_0 \left[ \sinh(n\pi d/a) + \epsilon_r \cosh(n\pi d/a) \right]}} \quad \dots 2.19$$

Now to find the effective dielectric constant, we consider two cases of capacitance:

Let  $C =$  capacitance per unit length of the micro strip line with a dielectric substrate ( $\epsilon_r \neq 1$ )

Let  $C_0 =$  capacitance per unit length of the micro strip line with an air dielectric ( $\epsilon_r = 1$ )

Since capacitance is proportional to the dielectric constant of the material homogeneously filling the region around the conductors, we have that

$$\epsilon_e = \frac{C}{C_0} \quad \dots 2.20$$

So (2.20) can be evaluated by computing (2.19) twice; once with  $\epsilon_r$  equal to the dielectric constant of the substrate (for  $C$ ), and then with  $\epsilon_r = 1$  (for  $C_0$ ). The characteristic impedance is then



$$Z_0 = \frac{1}{v_p C} = \frac{\sqrt{\epsilon_e}}{cC} \quad \dots 2.21$$

Where  $c = 3 \times 10^8 \text{ m/sec}$ .

## CHAPTER -3

### BASIC CONCEPTS AND THEORIES OF FILTER

#### 3.1 General Definitions

The transfer function of a two-part filter network is a mathematical description of network response characteristic, namely, a mathematical expression of  $S_{21}$ . On many occasions, an amplitude-squared transfer function for a lossless passive filter network is defined as

$$|S_{21}(j\Omega)|^2 = \frac{1}{1 + \epsilon^2 F_n^2(\Omega)} \quad \dots (1)$$

Where  $\epsilon$  is a ripple constant,  $F_n(\Omega)$  represents a filtering or characteristic function, and  $\Omega$  is a frequency variable of a low pass prototype filter that has a cutoff frequency at  $\Omega = \Omega_c$  for  $\Omega_c = 1$  (rad/s). Frequency transformations to the usual radian frequency for practical low pass, high pass, bandpass and band stop filters will be discussed later on.

For linear, time-invariant networks, the transfer function may be defined as a rational function, that is

$$S_{21}(\rho) = \frac{N(\rho)}{D(\rho)} \quad \dots (2)$$

Where  $N(\rho)$  and  $D(\rho)$  are polynomials in a complex frequency variable  $p = \sigma + j\Omega$ . For a lossless passive network, the neper frequency  $\sigma = 0$  and  $p = j\Omega$ . To find a realizable rational transfer function that produces response characteristics approximating the required response is the so-called approximation problem, and in many cases, the rational transfer function of (2) can be constructed from the amplitude-squared transfer function of (1).

For a given transfer function of (1), the insertion loss response of the filter, following the conventional definition, can be computed by

$$L_A(\Omega) = 10 \log \frac{1}{|S_{21}(j\Omega)|^2} \text{ dB} \quad \dots (3)$$

Since  $|S_{11}|^2 + |S_{21}|^2 = 1$  for a lossless, passive two-port network, the return loss response of the filter can be found as

$$L_R(\Omega) = 10 \log [1 - |S_{21}(j\Omega)|^2] \quad \dots (4)$$

If a rational transfer function is available, the phase response of the filter can be found as

$$\Phi_{21} = A_{rg} S_{21}(j\Omega) \quad \dots (5)$$

Then the group delay response of this network can be calculated by

$$\tau_d(\Omega) = \frac{d\Phi_{21}(\Omega)}{-d\Omega} \text{ Seconds} \quad \dots (6)$$

Where  $\Phi_{21}(\Omega)$  is in radians and is in radians per second.

### 3.2 The Poles and Zeros on the Complex Plane

The  $(\sigma, \Omega)$  plane, where a rational transfer function is defined, is called the complex plane or the  $p$ -plane. The horizontal axis of this plane is called the real or  $\sigma$ -axis, and the vertical axis is called the imaginary or  $j\Omega$ -axis. The values of  $p$  at which the function becomes zero are the zeros of the function, and the values of  $p$  at which the function becomes infinite are the singularities (usually the poles) of the function. Therefore, the zeros of  $S_{21}(p)$  are the roots of the numerator  $N(p)$  and the poles of  $S_{21}(p)$  are the roots of denominator  $D(p)$ .

These poles will be the natural frequencies of the filter whose response is described by  $S_{21}(p)$ . For the filter to be stable, these natural frequencies must lie in the left half of the  $p$ -plane, or on the imaginary axis. If this were not so, the oscillations would be of exponentially increasing magnitude with respect to time, a condition that is impossible in a passive network. Hence,  $D(p)$  is a Hurwitz polynomial i.e. its roots (or zero's) are in the inside of the left half-plane, or on the  $j\Omega$ -axis, whereas the roots (or zero's) of  $N(p)$  may occur anywhere on the entire complex plane. The zeros of  $N(p)$  are called finite-frequency transmission zeros of the filter.

The poles and zeros of a rational transfer function may be depicted on the  $p$ -plane. We will see in the following the different types of transfer functions will be distinguished from their pole-zero patterns of the diagram.

### 3.3 Butterworth (Maximally Flat) Response

The amplitude-squared transfer function for Butterworth, filters that have an insertion loss  $L_{Ay}=3.01$  dB at the cutoff frequency  $\Omega_c=1$  is given by

$$|S_{21}(j\Omega)|^2 = \frac{1}{1+\Omega^{2n}} \quad \dots (7)$$

Where  $n$  is the degree or the order of filter, which corresponds to the number of reactive elements required in the low pass prototype filter. This type of response is also referred to as maximally flat because its amplitude-squared transfer function defined in (7) has the maximum number of  $(2n - 1)$  zero derivatives at  $\Omega=0$ . Therefore, the maximally flat approximation on the ideal low pass filtering the pass-band is best at  $\Omega=0$ , but deteriorates as  $\Omega$  approaches the cutoff frequency  $\Omega_c$ . Figure 3.1 shows a typical maximally flat response.

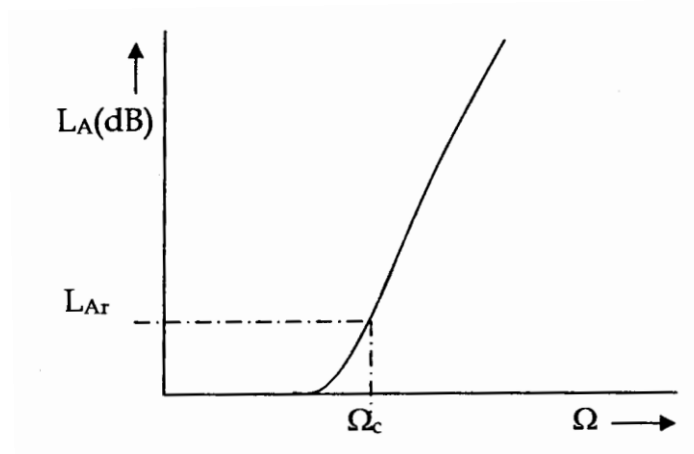


Fig. 3.1. Butterworth (maximally flat) low pass response

A rational transfer function constructed from (7) is

$$S_{2_1}(p) = \frac{1}{\prod_{i=1}^n (P - P_i)} \quad \dots (8)$$

With  $P_i = j \exp\left\{ \frac{(2i-1)\pi}{2\pi} \right\}$

There is no finite-frequency transmission zero [all the zeros of  $S_{2_1}(p)$  are at infinity], and the poles  $p_i$ , lie on the unit circle in the left half-plane at equal angular spacing, since  $|p_i|=1$  and  $\text{Arg } p_i = \frac{(2i-1)\pi}{2\pi}$ . This is illustrated in Figure 3.2.

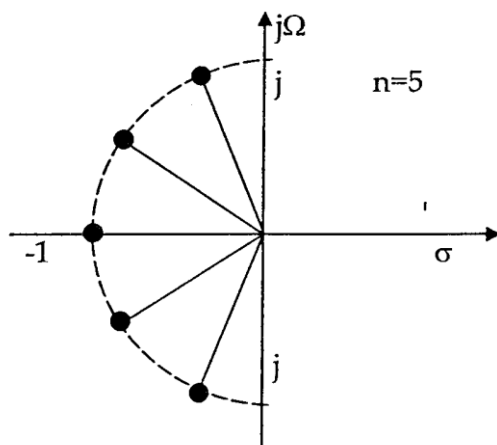


Fig. 3.2. Pole distribution for Butterworth (maximally flat) response.

Figure 3.2 plots the two typical oscillating curves for  $n=4$  and  $n=5$ . An important property of this is that if  $\Omega_c$  can be found such that  $F_n(\Omega_c)$  has equal ripples in the passband, it will automatically have equal ripples in the stopband. The parameter  $\Omega_c$  is the frequency at which the equal-ripple stopband starts. For  $n$  even  $F_n(\Omega_c) = M$  is required, which can be used to define the minimum in the stopband for a specified passband ripple constant  $\epsilon$ .

The transfer function can lead to expressions containing elliptic functions; for this reason, filters that display such a response are called elliptic function filters, or simply elliptic filters. They may also occasionally be referred to as Cauer filters, after the person who first introduced the function of this type.

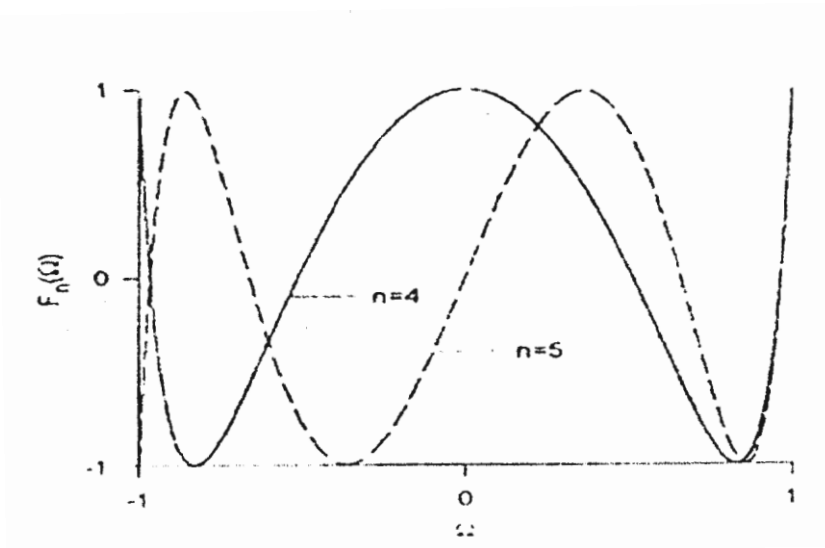


Fig. 3.3 : Plot of elliptic rational function.

### 3.4 Gaussian (Maximally Flat Group-Delay) Response

The Gaussian response is approximated by a rational transfer function

$$S_{2_1}(p) = \frac{a_0}{\sum_{k=0}^n a_k p^k} \quad \dots (9)$$

Where  $p = \sigma + j\Omega$  is the normalized complex frequency variable, and the coefficients

$$a_k = \frac{(2n-k)}{2^{n-k} k!(n-k)!} \quad \dots (10)$$

This transfer function possess a group delay that has maximum possible number of zero derivatives with respect to  $\Omega$  at  $\Omega=0$ , which is why it is said to have maximally flat group delay around  $\Omega=0$  and is in a sense complementary to the Butterworth response, which has a maximally flat amplitude. The above maximally flat group delay approximation was originally derived by W. E. Thomson. The resulting polynomials in (9) are related to the Bessel functions. For these reasons, the filters of this type are also called Bessel and or Thompson filters.

Figure 3.4 shows two typical Gaussian responses for  $n=3$  and  $n=5$ , which are obtained from (9). In general, the Gaussian filters have a poor selectivity, as can be seen from the amplitude responses in Figure 3(a). With increasing filter order  $n$ , the selectivity improves group delay little.

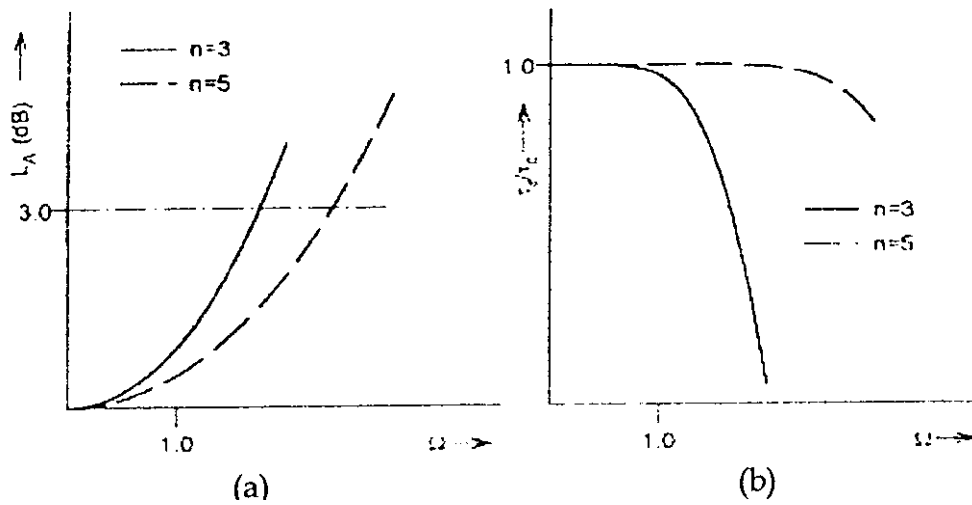


Fig. 3.4 : Gaussian (maximally flat group-delay) response : (a) amplitude (b) and the insertion loss in decibels approaches the Gaussian form

$$L_A(\Omega) = 10 \log e^{\frac{\Omega^2}{(2n-1)}} \text{ dB} \quad \dots (11)$$

Use of this equation gives the 3 dB bandwidth as

$$\Omega_{3dB} = \sqrt{(2n-1) \ln 2} \quad \dots (12)$$

Which approximation is good for  $n \geq 3$ . Hence unlike the Butterworth response, the 3 dB bandwidth of a Gaussian filter is a function of the filter order; the higher the filter order, the wider the 3 dB bandwidth.

However, the Gaussian filters have a quite flat group delay in the passband, as indicated in Figure 3(b), where the group delay is normalized by  $\tau_0$ , which is the delay at the zero frequency and is inversely proportional to the bandwidth of the passband. If we let  $\Omega_0 = \Omega_0 = 1$  radian per second be a reference bandwidth, then  $\tau_0 = 1$  second. With increasing filter order  $n$ , the group delay is flat over a wider frequency range. Therefore, a high-order Gaussian filter is usually used for achieving a flat group delay over a large passband.

### 3.5 All-Pass Response

External group delay equalizers, which are realized using all-pass networks, are widely used in communications systems. The transfer function of an all-pass network is defined as

$$S_{21} = \frac{D(-p)}{D(p)} \quad \dots (13)$$

Where  $p = \sigma + j\Omega$  is the complex frequency variable and  $D(p)$  is a strict Hurwitz polynomial. At real frequencies ( $p = j\Omega$ ),  $|S_{21}(j\Omega)|^2 = S_{21}(p)S_{21}(-p) = 1$  so that the amplitude response is unity at all frequencies, which is why it is called the all-pass network. However, there will be phase shift and group delay produced by the all-pass network. We may express (13) at real frequencies as  $S_{21}(j\Omega) = e^{j\Phi_{21}(\Omega)}$ , the phase shift of an all-pass network is then

$$\Phi_{21}(\Omega) = -j \ln S_{21}(j\Omega) \quad \dots (14)$$

and the group delay is given by

$$\begin{aligned} \tau_d(\Omega) &= \frac{d\Phi_{21}(\Omega)}{d\Omega} = j \frac{d(\ln S_{21}(j\Omega))}{d\Omega} \\ &= j \left( \frac{1}{D(-p)} \frac{dD(-p)}{dp} - \frac{1}{D(p)} \frac{dD(p)}{dp} \right) \frac{dp}{d\Omega} \Big|_{p=j\Omega} \end{aligned} \quad \dots (15)$$

An expression for a strict Hurwitz polynomial  $D(p)$  is

$$D(p) = \left( \prod_{k=1}^n [p - (-\sigma_k)] \right) \left( \prod_{k=1}^m [p - (-\sigma_i + j\Omega_i)] [p - (-\sigma_i - j\Omega_i)] \right) \quad \dots (16)$$

where  $-\sigma_k$  for  $\sigma_k > 0$  are the real left-hand roots, and  $-\sigma_i = j\Omega_i$  for  $\sigma_i > 0$  and  $\Omega_i > 0$  are the complex left-hand roots of  $D(p)$ , respectively. If all poles and zeros of an all-pass network are located along the  $-$ axis, such a network is said to consist of C-type sections and therefore referred to as C-type all-pass network. On the other hand, if the poles and zeros of the transfer function in (13) are all complex with quadrantile symmetry about the origin of the complex plane, the resultant network is referred to as D-type all-pass network consisting of D-type sections only. In practice, a desired all-pass network may be constructed by a cascade connection of individual C-type and D-type sections. Therefore, it is interesting to discuss their characteristics separately.

For a single section C-type all-pass network, the transfer function is

$$S_{21}(p) = \frac{-p + \sigma_k}{p + \sigma_k} \quad \dots (17)$$

and the group delay found by (15) is

$$T_d(\Omega) = \frac{2\sigma_k}{\sigma_k^2 + \Omega^2} \quad \dots (18)$$

The pole-zero diagram and group delay characteristics of this network are illustrated in Figure 3.5.

Similarly, for a single-section, D-type, all-pass network, the transfer function is

$$S_{21}(p) = \frac{[-p - (-\sigma_1 + j\Omega_1)] \cdot [-p - (-\sigma_1 - j\Omega_1)]}{[p - (-\sigma_1 + j\Omega_1)] \cdot [p - (-\sigma_1 - j\Omega_1)]} \quad \dots (19)$$



and the group delay is

$$T_d(\Omega) = \frac{4\sigma_1 [(\sigma_1^2 + \Omega_1^2) + \Omega^2]}{[(\sigma_1^2 + \Omega_1^2) + \Omega^2]^2 + (2\sigma_1\Omega)^2} \dots (20)$$

Figure 3.5 depicts the pole-zero diagram and group delay characteristics of this network.

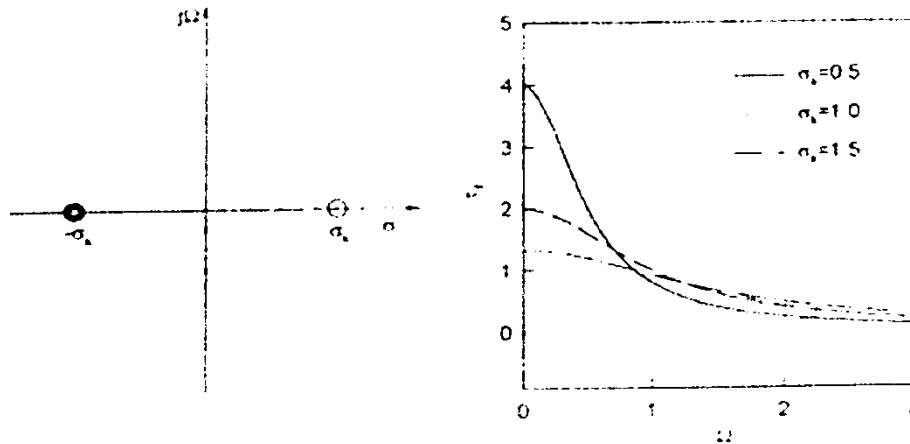


Fig. 3.5 : Characteristics of single-section C-type all-pass network : (a) pole zero diagram (b) group delay response.

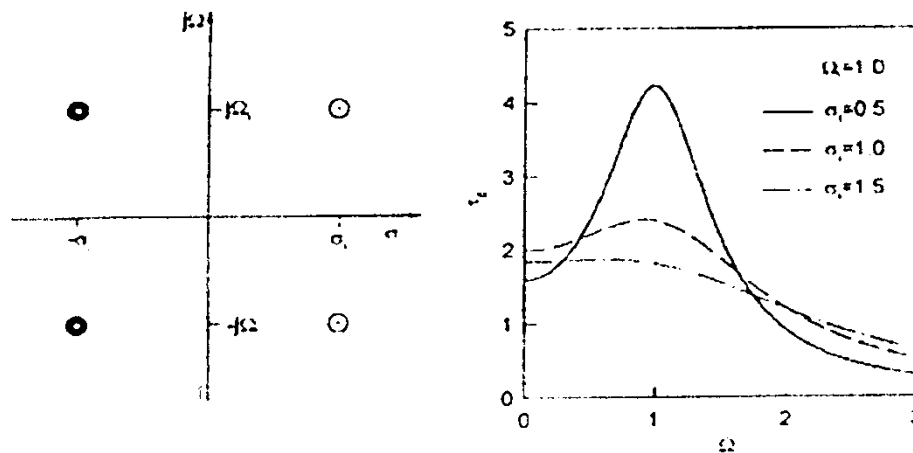


Fig. 3.6 : Characteristics of single-section D-type, all-pass network : (a) pole zero diagram (b) group delay response.

### 3.7 Elliptic Function Low pass Prototype Filters

Figure 7 illustrates two commonly used network structures for elliptic function low pass prototype filters. In figure 7(a), the series branches of parallel-resonant circuits are introduced for realizing the finite-frequency transmission zeros, since they block transmission by having infinite series impedance (open-circuit) at resonance. For this form of the elliptic function low pass prototype,  $g$ : for odd  $i(i = 1, 3, \dots)$  represent the capacitance of a shunt capacitor,  $g$  : for even  $i(i = 2, 4, \dots)$  represent the inductance of an inductor, and the primed  $g$  : for even  $i(i = 2, 4, \dots)$  are the capacitance of a capacitor in a series branch of parallel-resonant circuit. For the dual realization form in Figure 7(b), the shunt branches of series-resonant circuits are used for implementing the finite-frequency transmission zeros, since they short out transmission at resonance. In this case, referring to Figure 7(b),  $g$ : for odd  $i(i = 1, 3, \dots)$  are the inductance of a series inductor,  $g$ : for odd  $i(i = 2, 4, \dots)$  are the capacitance of a capacitor, and primed  $g$ : for

even  $i(i = 2, 4, \dots)$  indicate the inductance of an inductor in a shunt branch of series-resonant circuit. Again, either form may be used, because both give the same response.

### 3.8 Low pass Transformation

The frequency transformation from a low pass to a practical low pass filter having a cutoff frequency  $\omega_c$  in the angular frequency axis is simply given by

$$\Omega = \left( \frac{\Omega_c}{\omega_c} \right) \omega \quad \dots (21)$$

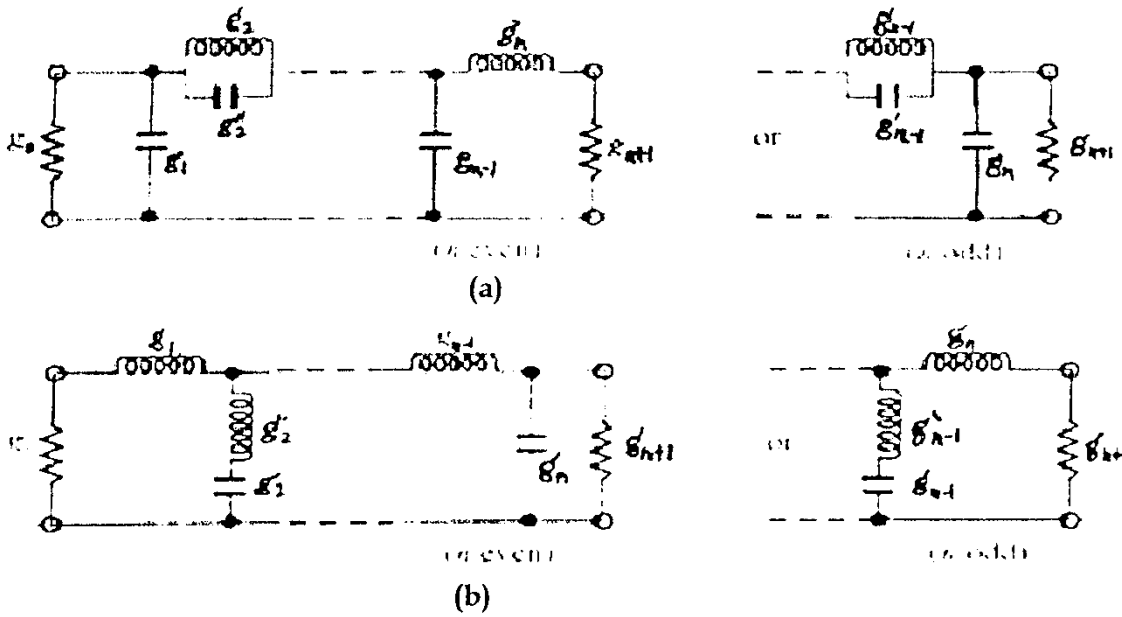


Fig. 3.7 : Low pass prototype filters for elliptic function filters with (a) series parallel-resonant branches, (b) its dual with shunt series-resonant branches.

Applying (21) together with the impedance scaling described above yields the element transformation:

$$L = \left( \frac{\Omega_c}{\omega_c} \right) y_0 g \quad \text{For } g \text{ representing the inductance}$$

$$C = \left( \frac{\Omega_c}{\omega_c} \right) \frac{g}{y_0} \quad \text{For representing the capacitance} \quad \dots (22)$$

Which is shown in Figure 8(a). To determine the use of the element transformation, let us consider design of a practical low pass filter with a cutoff frequency  $f_c=2GHz$  and a source impedance  $Z_0=50\Omega$ . A 3-pole Butterworth low pass prototype with the structure is chosen for this example, which gives  $g_0 = g_4 = 1.0mhos$ ,  $g_1 = g_2 = 1.0H$  and for  $\Omega_c = 1.0 \frac{rad}{s}$ . The impedance scaling factor is  $\gamma_0 = 50$ . The angular cutoff frequency  $\omega_c = 2\pi \times 2 \times 10^9 \frac{rad}{s}$ . We find  $L_1 = L_2 = 3.979nH$  and  $C_2 = 3.183pF$ . The resultant low pass filter is illustrated in Figure 3.8(b).

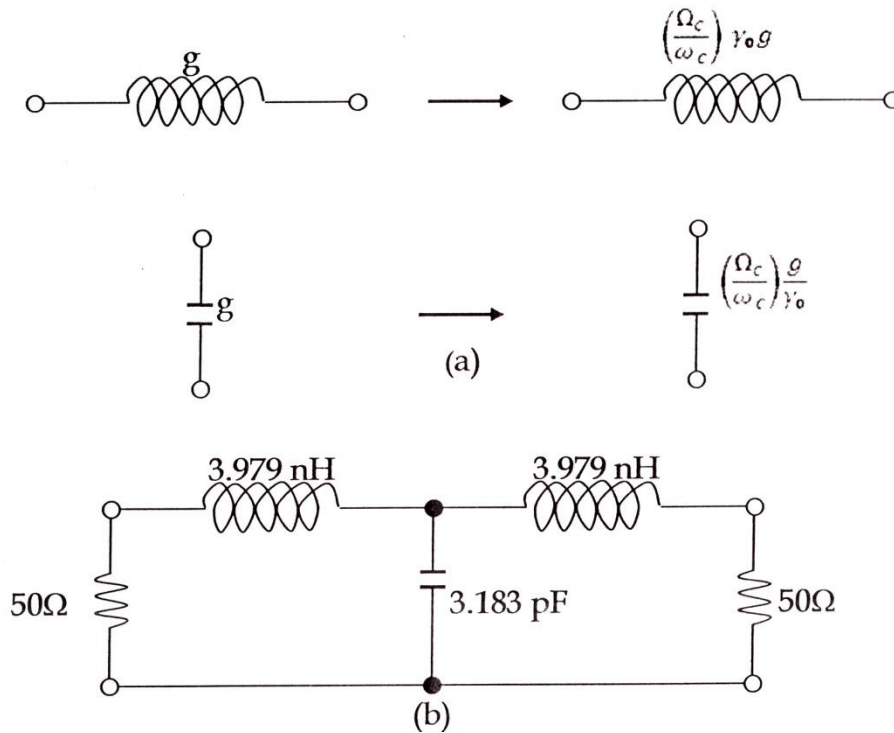


Fig. 3.8 : Low pass prototype to low pass transformation : (a) basic element transformation,(b) a practical low pass filter based on the transformation.

### 3.9 Filters with Immittance Inverters

It can be shown by network analysis that a series inductance with an inverter on each side looks like a shunt capacitance from its exterior terminals, as indicated in Figure 9(a). Likewise, a shunt capacitance with an inverter on each side looks like a series inductance from its external terminals, as demonstrated in Figure 9(b). Also as indicated inverters have the ability to shift impedance or admittance levels depending on the choice of K or J parameters. Making use of these properties enables us to convert a filter circuit to an equivalent form that would be more convenient for implementation with microwave structures.

For example, the two common low pass prototype structures may be converted into the forms shown in Figure 10, where the  $g$ : values are the original prototype element values as defined before. The new element values, such as  $Z_0, Z_{g+1}, L_{g1}, Y_e, Y_{g+1}$  and  $C_0$  may be chosen arbitrarily and the filter response will be identical to that of the original prototype, provided that the Immittance inverter parameters  $K_{i,i+1}$  and  $J_{i,i+1}$  are specified as indicated by the equations in Figure 10. These equations can be derived by expanding the input Immittance of the original

prototype networks and the equivalent ones in continued fractions and by equating corresponding terms.

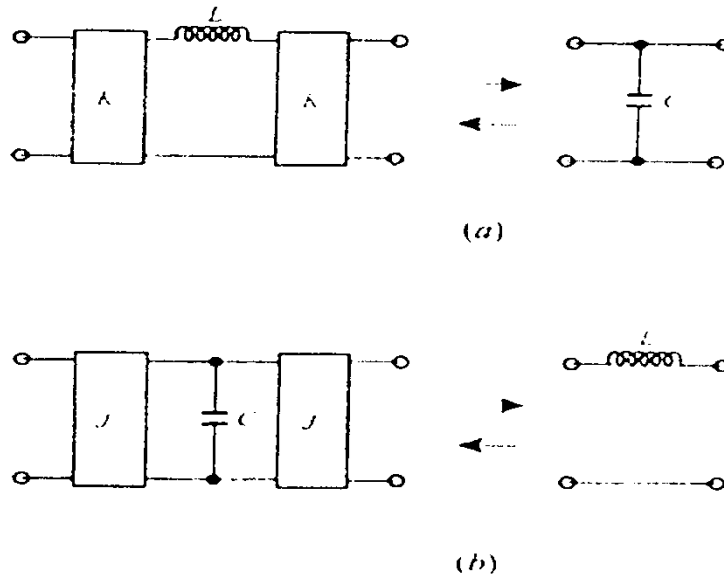


Fig. 3.9 : (a) Immittance inverters used to convert a shunt capacitance into an equivalent circuit with series inductance (b) Immittance inverters used to convert a series inductance into an equivalent circuit with shunt capacitance.

Since, ideally, Immittance inverter parameters are frequency invariable, the low-pass filter networks in Figure 10 can easily be transformed to other types of filters by applying the element transformations similar to those described in the previous section. For instance, Figure 11 illustrates two bandpass filters using Immittance inverters. In the case of Figure 3.11(a), only series resonators are involved, whereas the filter in Figure 3.11(b) consists of only shunt parallel resonators. The element transformations from Figure 3.10(a) to Figure 3.10(a) are

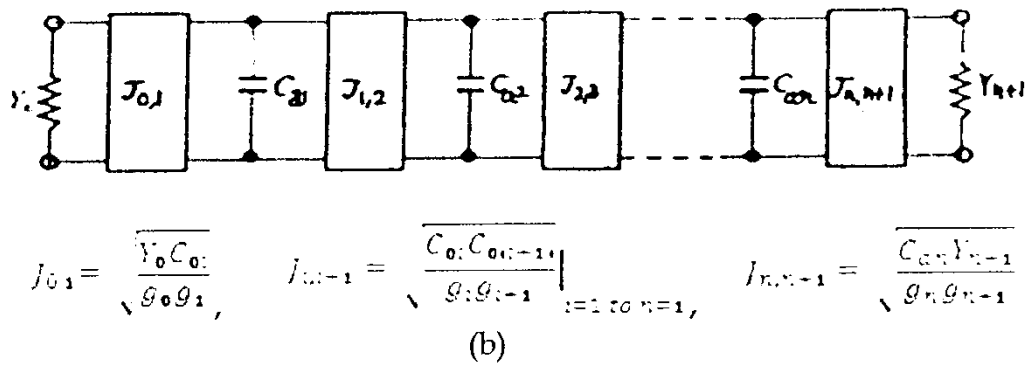
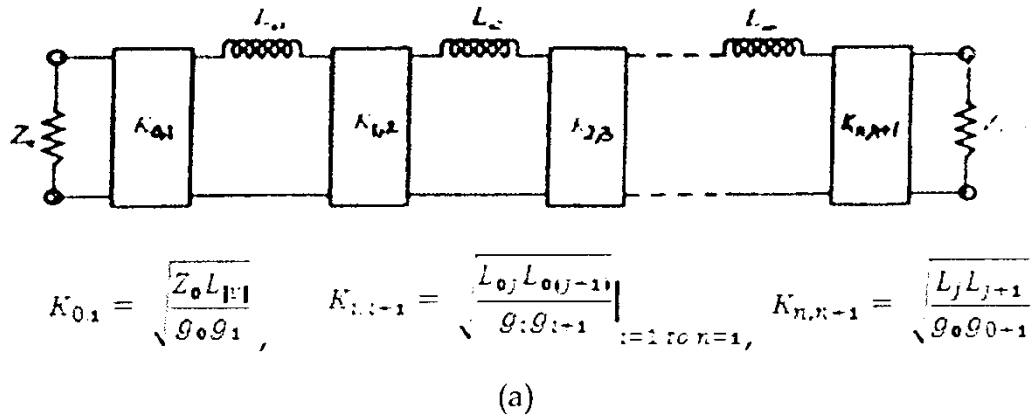


Fig. 3.10: Low pass prototype filters modified to include Immittance inverter obtained as follows. Since the source impedances are assumed the same in the both filters as indicated, no impedance scaling is required and the scaling factor  $Y_0 = 1$ . Now, viewing  $L_{\alpha 1}$  as inductive  $g$ , and transforming the inductors of the low pass filter to the series resonators of the bandpass filter, we obtain

$$L_{S1} = \left( \frac{\Omega_c}{FBW \omega_e} \right) L_{\alpha 1}$$

$$C_{S1} = \frac{1}{\omega_0^2 L_{S1}}$$

As mentioned above, the  $K$  parameters must remain unchanged with respect to the frequency transformation. Replacing  $L_{\alpha 1}$  in the equations in Figure 10(a) with  $L_{\alpha 1} = \left( \frac{FBW \omega_e}{\Omega_c} \right) L_{S1}$  yields the equations in Figure 10(a). Similarly the transformations and equations in Figure 11(b) can be obtained on a dual basis.

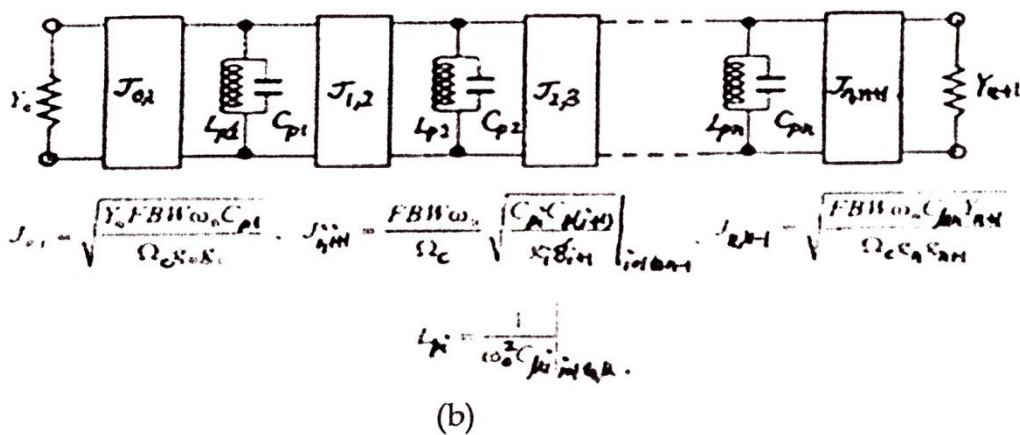
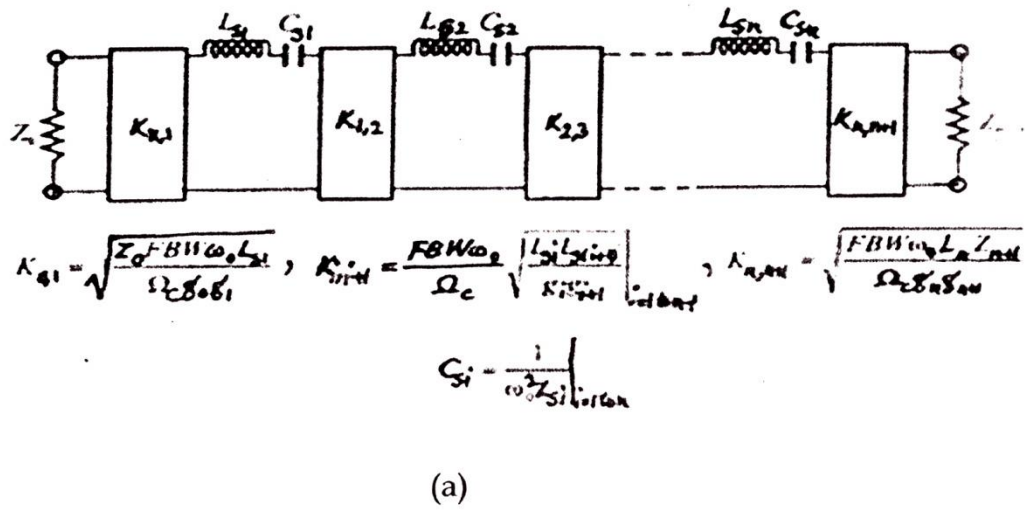


Fig. 3.11 : Bandpass filters using Immittance inverters.

Two important generalizations, shown in Figure 3.11, are obtained by replacing the lumped LC resonators by distributed circuits. Distributed circuits can be microwave cavities, micro strip resonators or any other suitable resonant structures. In the ideal case, the reactance's or susceptances of the distributed circuits (not restricted to bandpass filters) should equal those of the lumped resonators at all frequencies. In practice, they approximate the reactance's or susceptances of the lumped resonators only near resonance. Nevertheless, this is sufficient for narrow band filters. For convenience, the distributed resonator reactance/susceptances and reactance/susceptances slope are made equal to their corresponding lumped-resonator values at band center. For this, two quantities, called the reactance slope parameter and susceptances slope parameter, respectively, are introduced. The reactance slope parameter for resonators having zero reactance at center frequency  $\omega_c$  is defined by

$$X = \frac{\omega_0}{2} \left. \frac{dX(\omega)}{d\omega} \right|_{\omega=\omega_0} \dots (23)$$

Where  $X(\omega)$  is the reactance of the distributed resonator? In the dual case, the susceptances slope parameter for resonators having zero susceptances at center frequency  $\omega_c$  is defined by



$$B = \frac{\omega_0}{2} \left. \frac{dB(\omega)}{d\omega} \right|_{\omega=\omega_0} \dots (24)$$

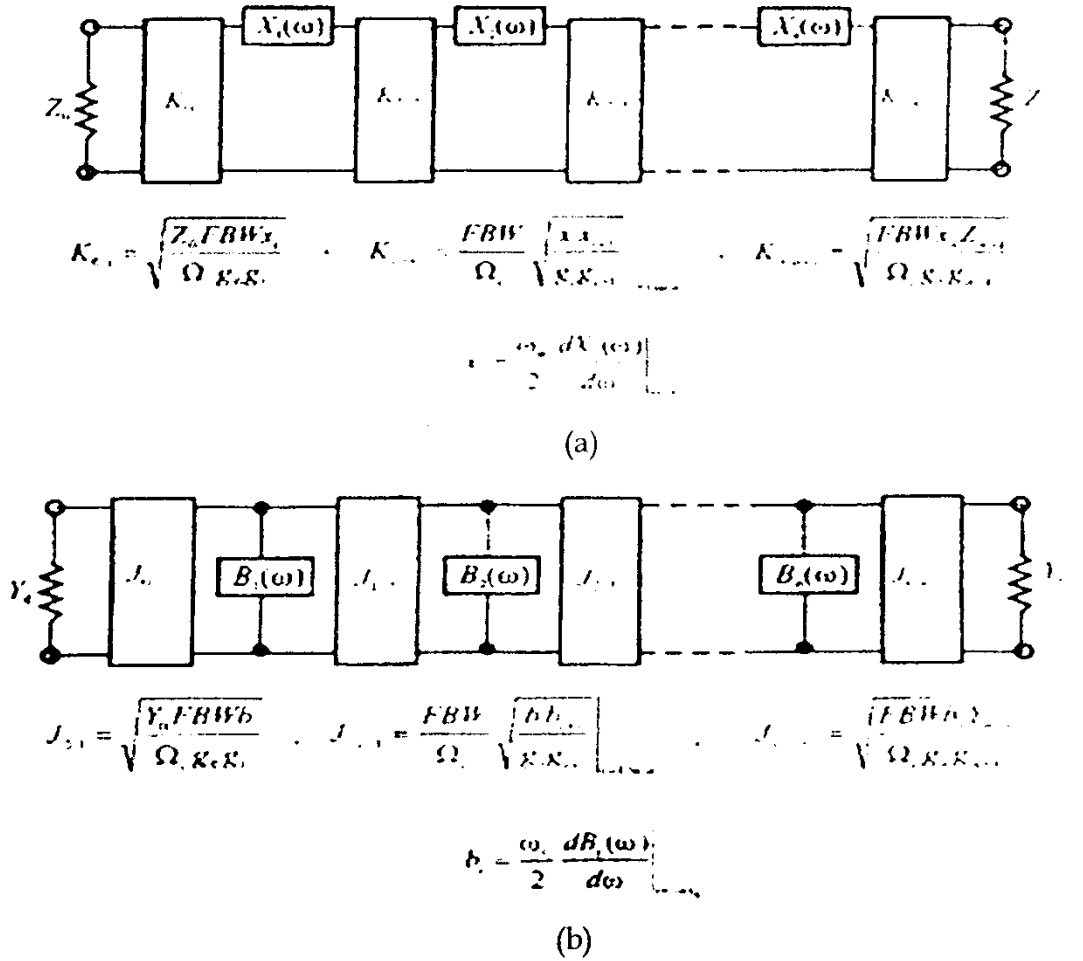


Fig. 3.12 : Generalized bandpass filters (including distributed elements) using Immittance inverters.

Where  $B(\omega)$  is the susceptances of the distributed resonator. It can be shown that the reactance slope parameter of a lumped LC series resonator is  $\omega_0 L$  and the susceptances slope parameters of a lumped LC parallel resonator is  $\omega_0 C$ . Thus, replacing  $\omega_0 L_{s1}$  and  $C_{p1}$  in the equations in Figure 9 with the general terms  $x_1$  and  $b_1$  as defined by (23) and (24), respectively, results in the equations indicated in Figure 3.12.

## CHAPTER -4

### WORKING PRINCIPLE OF HFSS & CST

I have studied the analysis of Micro strip Phase Bridge using two software's namely CST and HFSS. CST works on Finite Integration Technique (FTT) and HFSS works on Finite Element Method (FEM).

#### 4.1 FINITE ELEMENT METHOD (FEM)

The finite element method (FEM) (sometimes referred to as finite element analysis) is a numerical technique for finding approximate solutions of partial differential equations (PDE) as well as of integral equations. The solution approach is based either on eliminating the differential equation completely (steady state problems), or rendering the PDE into an approximating system of ordinary differential equations, which are then numerically integrated using standard techniques such as Euler's method, Runge-Kutta, etc. In solving partial differential equations, the primary challenge is to create an equation that approximates the equation to be studied, but is numerically stable, meaning that errors in the input data and intermediate calculations do not accumulate and cause the resulting output to be meaningless. There are many ways of doing this, all with advantages and disadvantages. The Finite Element Method is a good choice for solving partial differential equations over complex domains (like cars and oil pipelines), when the domain changes (as during a solid state reaction with a moving boundary), when the desired precision varies over the entire domain, or when the solution lacks smoothness. For instance, in a frontal crash simulation it is possible to increase prediction accuracy in "important" areas like the front of the car and reduce it in its rear (thus reducing cost of the simulation); Another example would be the simulation of the weather pattern on Earth, where it is more important to have accurate predictions over land than over wide-open sea.

#### 4.2 Technical discussion

We will illustrate the finite element method using two sample problems from which the general method can be extrapolated. It is assumed that the reader is familiar with calculus and linear algebra. P1 is a one-dimensional problem

$$P1 : \begin{cases} u'' = f \text{ in } (0,1) \\ u(0) = u(1) = 0 \end{cases} \quad \dots 4.1$$

Where  $f$  is given and  $u$  is an unknown function of  $x$ , and  $u''$  is the second derivative of  $u$  with respect to  $x$ . The two-dimensional sample problem is the Dirichlet problem

$$P2 : \begin{cases} u_{xx} + u_{yy} = f & \text{in } \Omega \\ u = 0 & \text{on } \partial\Omega \end{cases} \quad \dots 4.2$$

Where  $\Omega$  is a connected open region in the  $(x, y)$  plane whose boundary is "nice" (e.g., a smooth manifold or a polygon), and  $u_{xx}$  and  $u_{yy}$  denote the second derivatives with respect to  $x$  and

y, respectively. The problem P1 can be solved "directly" by computing antiderivatives. However, this method of solving the boundary value problem works only when there is only one spatial dimension and does not generalize to higher-dimensional problems or to problems like  $u + u'' = f$ . For this reason, we will develop the finite element method for P1 and outline its generalization to P2. Our explanation will proceed in two steps, which mirror two essential steps one must take to solve a boundary value problem (BVP) using the FEM.

- In the first step, one rephrases the original BVP in its weak, or variational form. Little to no computation is usually required for this step, the transformation is done by hand on paper.
- The second step is the discretization, where the weak form is discretized in a finite dimensional.

After this second step, we have concrete formulae for a large but finite dimensional linear problem whose solution will approximately solve the original BVP. This finite dimensional problem is then implemented on a computer.

### 4.3 Variational formulation

The first step is to convert P1 and P2 into their variational equivalents, or Weak formulation. If  $u$  solves P1, then for any smooth function  $v$  that satisfies the displacement boundary conditions, i.e.  $v = 0$  at  $x = 0$  and  $x = 1$ , we have

$$\int_0^1 f(x)v(x)dx = \int_0^1 u''(x)v(x)dx \quad \dots (1)$$

Conversely, if  $u$  with  $u(0) = u(1) = 0$  satisfies (1) for every smooth function  $v(x)$  then one may show that this  $u$  will solve P1. The proof is easier for twice continuously differentiable  $u$  (mean value theorem), but may be proved in a distributional sense as well. By using integration by parts on the right-hand-side of (1), we obtain

$$\begin{aligned} \int_0^1 f(x)v(x)dx &= \int_0^1 u''(x)v(x)dx \\ &= u'(x)v(x) \Big|_0^1 - \int_0^1 u'(x)v'(x)dx \quad \dots 4.3 \\ &= - \int_0^1 u'(x)v'(x)dx = -\Phi(u,v) \end{aligned}$$

where we have used the assumption that  $v(0) = v(1) = 0$

### 4.4 A proof outline of existence and uniqueness of the solution

We can loosely think of  $H_0^1(0,1)$  to be the absolutely continuous functions of  $(0,1)$  that are 0 at  $x = 0$  and  $x = 1$  (see Sobolev spaces). Such function are (weakly) "once differentiable" and it turns out that the symmetric bilinear map then defines an inner product which turns  $H_0^1(0,1)$  into a Hilbert space (a detailed proof is nontrivial). On the other hand, the left-hand-side

$\int_0^1 f(x)v(x)dx$  is also an inner product, this time on the  $L_p$  space  $L_2(0,1)$ . An application of the Riesz representation theorem for Hilbert spaces shows that there is a unique  $u$  solving (2) and therefore P1. This solution is a-priori only a member of, but using elliptic regularity, will be smooth if  $f$  is.

#### 4.5 The variational form of P2

If we integrate by parts using a form of Green's theorem, we see that if  $u$  solves P2, then for any  $v$ ,

$$\int_{\Omega} fv ds = - \int_{\Omega} \nabla u \cdot \nabla v ds = -t(u,v) \quad \dots 4.4$$

Where  $\nabla$  denotes the gradient and  $\cdot$  denotes the dot product in the two-dimensional plane. Once more can be turned into an inner product on a suitable space of "once differentiable" functions of that are zero on. We have also assumed that (see Sobolev spaces). Existence and uniqueness of the solution can also be shown.

#### 4.6 Discretization

The basic idea is to replace the infinite dimensional linear problem:

$$\begin{aligned} \text{Find } u \in H_0^1 \text{ such that} \\ \forall v \in H_0^1, -\Phi(u,v) = \int fv \end{aligned} \quad \dots 4.5$$

With a finite dimensional version:

$$\begin{aligned} \text{Find } u \in V \text{ such that} \\ \forall v \in V, -\Phi(u,v) = \int fv \end{aligned} \quad \dots 4.6$$

Where  $V$  is a finite dimensional subspace of  $H_0^1$ . There are many possible choices for  $V$  (one possibility leads to the spectral method). However, for the finite element method we take  $V$  to be a space of piecewise linear functions. For problem P1, we take the interval  $(0,1)$ , choose  $n$  values of  $x$  with  $0 = x_0 < x_1 < \dots < x_n < x_{n+1} = 1$  and we define  $V$  by

$V = \{v: [0,1] \rightarrow R: v \text{ is continuous, } v|_{[x_k, x_{k+1}]} \text{ is linear for}$

$$k = 0, \dots, n, \text{ and } v(0) = v(1) = 0\}$$

Where we define  $x_0 = 0$  and  $x_{n+1} = 1$ . Observe that functions in  $V$  are not differentiable according to the elementary definition of calculus. Indeed, if  $v \in V$  then the derivative is typically not defined at any  $x = x_k, k = 1, \dots, n$ . However, the derivative exists at every other value of  $x$  and one can use this derivative for the purpose of integration by parts.

For problem P2, we need  $V$  to be a set of functions of  $\Omega$ . In the figure on the right, we have illustrated a triangulation of 15 sided polygonal region  $\Omega$  in the plane (below), and a piecewise linear function (above, in color) of this polygon which is linear on each triangle of the

triangulation; the space  $V$  would consist of functions that are linear on each triangle of the chosen triangulation.

One often reads  $V_h$  instead of  $V$  in the literature. The reason is that one hopes that as the underlying triangular grid becomes finer and finer, the solution of the discrete problem (3) will in some sense converge the solution of the original boundary value problem  $P_2$ . The triangulation is then indexed by a real valued parameter  $h > 0$  which one takes to be very small. This parameter will be related to the size of the largest or average triangle in the triangulation. As we refine the triangulation, the space of piecewise linear functions  $V$  must also change with  $h$ , hence the notation  $V_h$ .

Since we do not perform such an analysis, we will not use this notation.

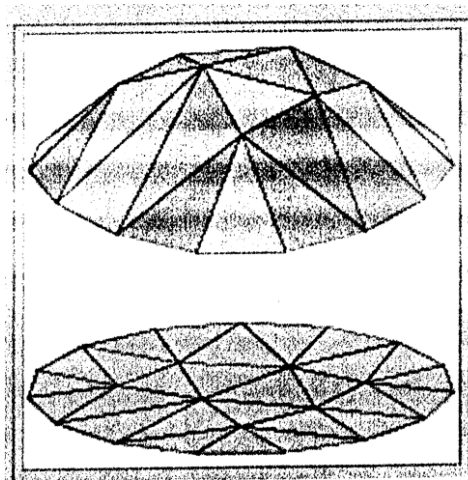


Fig. 4.1

### 4.7 Choosing a basis

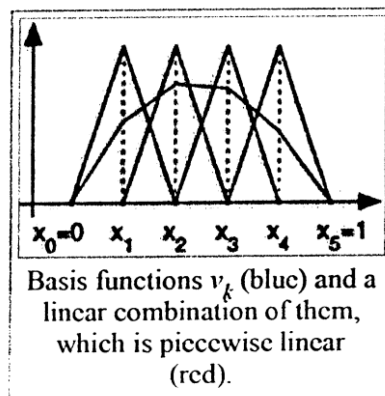


Fig. 4.2 choosing a basis function

To complete the discretization, we must select a basis of  $V$ . In the one-dimensional case, for each control point  $x_k$  we will choose the piecewise linear function  $v_k$  in  $V$  whose value is 1 at  $x_k$  and zero at every  $x_j, j \neq k$ , i.e.,

$$v_k(x) = \begin{cases} \frac{x - x_{k-1}}{x_k - x_{k-1}} & \text{if } x \in [x_{k-1}, x_k], \\ \frac{x_{k+1} - x}{x_{k+1} - x_k} & \text{if } x \in [x_k, x_{k+1}], \\ 0 & \text{otherwise,} \end{cases}$$

For  $k = 1, \dots, n$ ; this basis is a shifted and scaled tent function. For the two-dimensional case, we choose again one basis function  $v_k$  per vertex  $x_k$  of the triangulation of the planar region. The function  $v_k$  is the unique function of  $V$  whose value is 1 at  $x_k$  zero at every  $x_j, j \neq k$ .

Depending on the author, the word "element" in "finite element method" refers either to the triangles in the domain, the piecewise linear basis function, or both. So for instance, an author interested in curved domains might replace the triangles with curved primitives, in which case he might describe his elements as being curvilinear. On the other hand, some authors replace "piecewise linear" by "piecewise quadratic" or even "piecewise polynomial". The author might then say "higher order element" instead of "higher degree polynomial". Finite element method is not restricted to triangles (or tetrahedral in 3-d, or higher order simplexes in multidimensional spaces), but can be defined on quadrilateral sub domains (hexahedra, prisms, or pyramids in 3-d, and so on). Higher order shapes (curvilinear elements) can be defined with polynomial and even non-polynomial shapes (e.g. ellipse or circle). Examples of methods that use higher degree piecewise polynomial basis functions are the hp-FEM and spectral FEM. More advanced implementations (adaptive finite element methods) utilize a method to assess the quality of the results (based on error estimation theory) and modify the mesh during the solution aiming to achieve approximate solution within some bounds from the 'exact' solution of the continuum problem. Mesh adaptivity may utilize various techniques, the most popular are;

- 1) Moving nodes (r-adaptivity)
- 2) Refining (and unrefining) elements (h-adaptivity)
- 3) Changing order of base functions (p-adaptivity)
- 4) Combinations of the above (hp-adaptivity)

#### 4.8 FINITE INTEGRATION TECHNIQUE

CST MICROWAVE STUDIO is a general-purpose electromagnetic simulator based on the Finite Integration Technique (FIT), first proposed by Weiland in 1976/1977. This numerical method provides a universal spatial discretization scheme, applicable to various Electromagnetic problems, ranging from static field calculations to high frequency application in time or frequency domain. In the following section the main aspects of this procedure will be explained and afterwards extended to specialized forms concerning the different solver types.

Unlike most numerical methods, FIT discretizes the following integral form of Maxwell's equation, rather than the differential one:



$$\oint_{\partial A} \vec{E} \cdot d\vec{s} = - \int_A (\partial \vec{B} / \partial t) \cdot d\vec{A}$$

$$\oint_{\partial V} \vec{D} \cdot d\vec{A} = \int_V \rho dV$$

$$\oint_{\partial A} \vec{H} \cdot d\vec{s} = - \int_A ((\partial \vec{D} / \partial t) + \vec{J}) \cdot d\vec{A}$$

$$\oint_{\partial V} \vec{B} \cdot d\vec{A} = 0$$

In order to solve these equations numerically a finite calculation domain is defined, enclosing the considered application problem. By creating suitable mesh system, this domain is split up into several small cuboids, so-called grid cells. This *first* or *primary mesh* can be visualized in CST MICROWAVE STUDIO in the *Mesh View*, however, internally a *second* or *dual mesh* is set up orthogonally to the first one.

The spatial discretization of Maxwell's equations is finally performed on this two orthogonal grid systems, where the new degrees of freedom are introduced as integral values as well. Referring to the following picture, the electric grid voltages  $e$  and magnetic facet fluxes  $b$  are allocated on the primary grid  $G$  and the dielectric facet fluxes  $d$  as well as the magnetic grid voltages  $h$  on the dual grid  $G$  (indicated by the tilde):

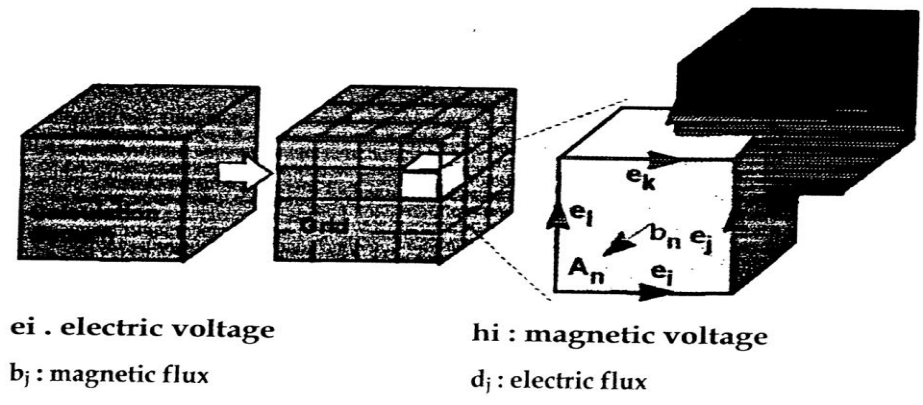


Fig. 4.3

Now Maxwell's equations are formulated for each of the cell facets separately as will be demonstrated in the following. Considering Faraday's law, the closed integral on the equation's left side can be rewritten as a sum of four grid voltages without introducing any supplementary errors. Consequently, the time derivative of the magnetic flux defined on the enclosed primary cell facet represents the right-hand side of the equation, as illustrated in the figure below. By repeating this procedure for all available cell facets, the calculation rule can be summarized in an elegant matrix formulation, introducing the topological matrix  $C$  as the discrete equivalent of the analytical curl operator:

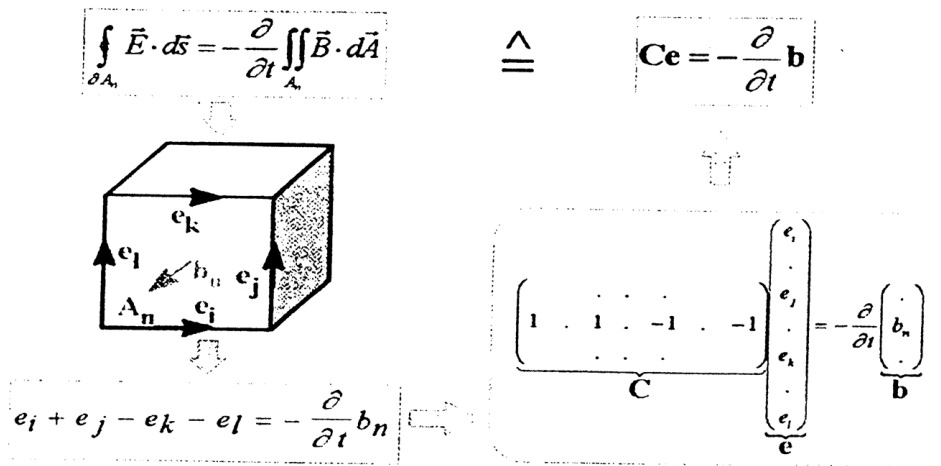


Fig. 4.4

Applying this scheme to Ampere's law on the dual grid involves the definition of a corresponding discrete curl operator C. Similarly the discretization of the remaining divergence equations (1b) introduces discrete divergence operators S and  $\tilde{S}$ , belonging to the primary and dual grid, respectively. As previously indicated, these discrete matrix operators just consist of elements '0', '1' and '-1', representing merely topological information. Finally we obtain the complete discretized set of the so-called *Maxwell's Grid Equations* (MGE's):

$$\begin{aligned}
 Ce &= -(db/dt) & \tilde{C}h &= (d/dt)d + j \\
 \tilde{S}d &= q & Sb &= 0
 \end{aligned}$$

Compared to the continuous form of Maxwell's equations, the similarity between both descriptions is obvious. Once again it should be mentioned that no additional error has yet been introduced. This essential point of FIT discretization is reflected in the fact that important properties of the continuous gradient, curl and divergence operation are still maintained in grid space:

$$\begin{aligned}
 SC = \tilde{S}\tilde{C} = 0 & \iff div\ rot = 0 \\
 C\tilde{S}^T = \tilde{C}S^T = 0 & \iff rot\ grad = 0
 \end{aligned}$$

At this point it should be mentioned that even the spatial discretization of a numerical algorithm could cause long term instability. However, based on the presented fundamental relations (3), it can be shown that the FIT formulation is not affected by such problems, since the set of MGE's (2) maintain energy and charge conservation [2].

Finally, the missing material equations introduce the inevitable numerical inaccuracy due to the spatial discretization. By defining the necessary relations between voltage and fluxes their integral values have to be approximated over the grid edges and cell areas, respectively. Consequently, the resulting coefficients depend on the averaged material parameters as well as on the spatial resolution of the grid and are summarized again in correspondent matrices:

$$\begin{aligned}
 \tilde{D} &= \epsilon\tilde{E} & d &= M_\epsilon e \\
 \tilde{B} &= \mu\vec{H} & \implies & b = M_\mu h \\
 \tilde{J} &= \sigma\tilde{E} + \tilde{j} & j &= M_\sigma e + j_s
 \end{aligned}$$

Now all matrix equations are available to solve electromagnetic field problems on the discrete grid space. The fact that the topological and metric information is divided into different equations has important theoretical, numerical and algorithmic consequences [2].

As demonstrated, the FIT formulation is a very general method and therefore can be applied to all frequency ranges, from DC to high frequencies (see figure below). All electromagnetic field regimes are already covered by CST's software package MAFIA®, whose development started more than 20 years ago.

Based on this long experience, the "STUDIO"-family development started in 1997. Here, several improvements concerning user interface, visualization and solver performance were integrated. However, the most fundamental change was the meshing strategy, the Perfect Boundary Approximation® (PBA) technique [3], particularly extended by the Thin Sheet Technique™ (TST) and the Multilevel Subgridding Scheme™ (MSS).

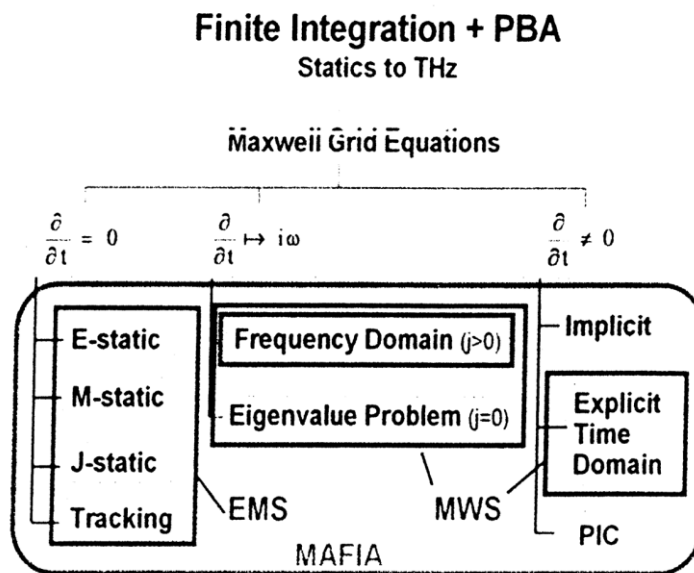


Fig. 4.5

Currently, there are two packages available: CST EM STUDIO™ (EMS), the low frequency package, which includes a variety of static and low frequency solvers and CST MICROWAVE STUDIO® (MWS), covering the high frequency range, both in transient and in harmonic state.

In the case of Cartesian grids, the FIT formulation can be rewritten in time domain to yield standard Finite Difference Time Domain methods (FDTD). However, whereas classical FDTD methods are limited to staircase approximations of complex boundaries, the PBA® technique applied to the FIT algorithm maintains all the advantages of structured Cartesian grids, while allowing an accurate modeling of curved structures.

In the figure below, the two "classical" geometry discretization are shown: the Finite Element Method model on the left and the FDTDrrLM model on the right. The FIT model together with the PBA® theory in the middle combines the advantages of the other two models. It offers both an excellent geometry approximation, without the segmentation of FE models and staircase approximation of FDTD codes, and high simulation speed, as in the FDTD and TLM methods.

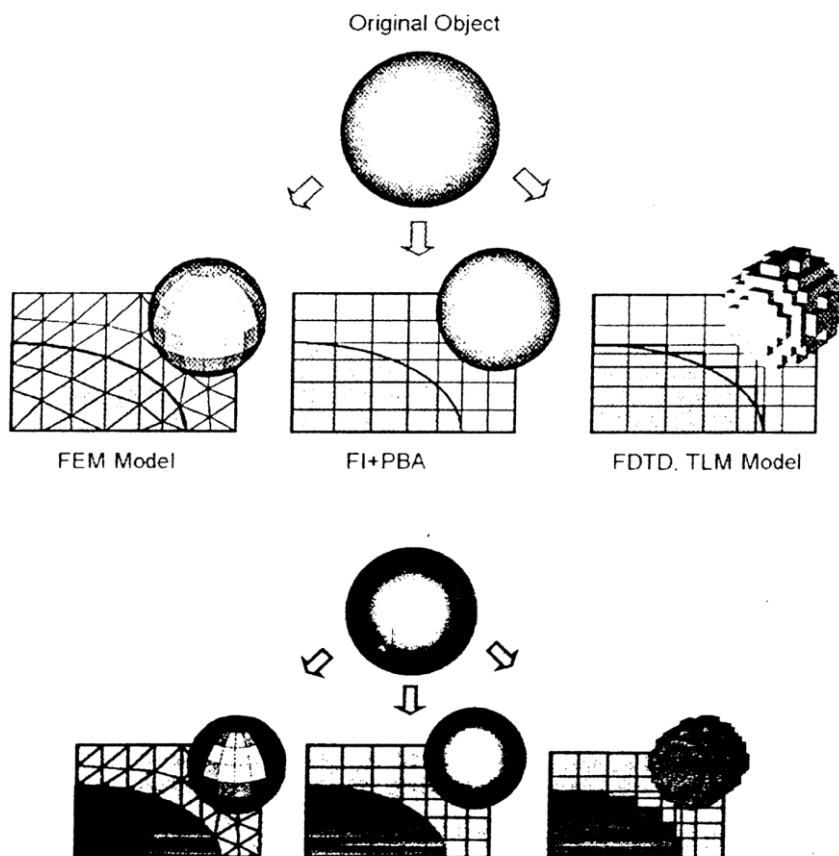
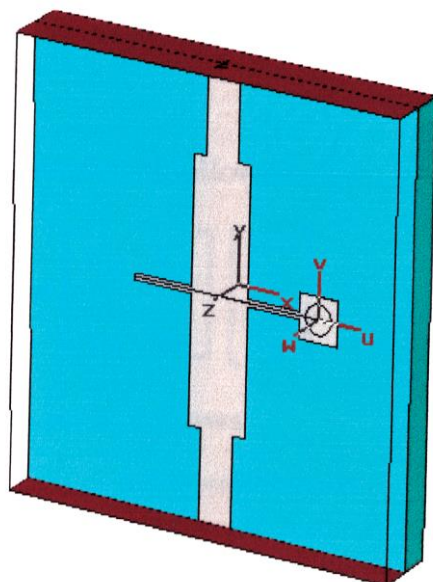
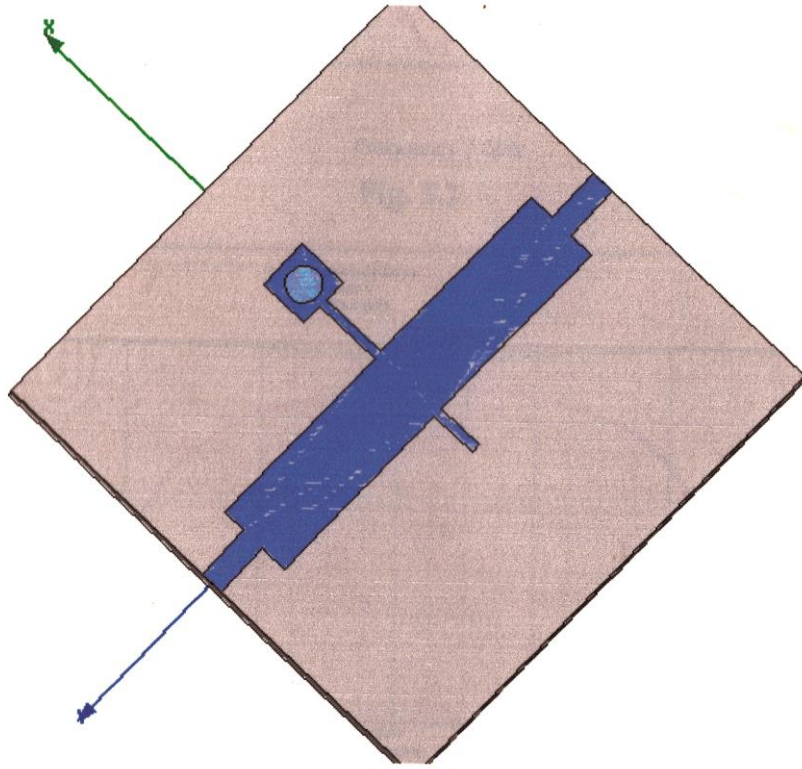


Fig. 4.6

**4.9 The Micro strip Phase Bridge/Shifter simulated on CST is given below**



and that on HFSS is shown below



## CHAPTER -5

### RESULTS

#### S-Parameters

The complete matrix representation follows:

$$\begin{bmatrix} V_2^- \\ V_2^- \end{bmatrix} = \begin{bmatrix} S_{22} & S_{22} \\ S_{22} & S_{22} \end{bmatrix} \begin{bmatrix} V_2^+ \\ V_2^+ \end{bmatrix}$$



### The HFSS and CST results are as follows

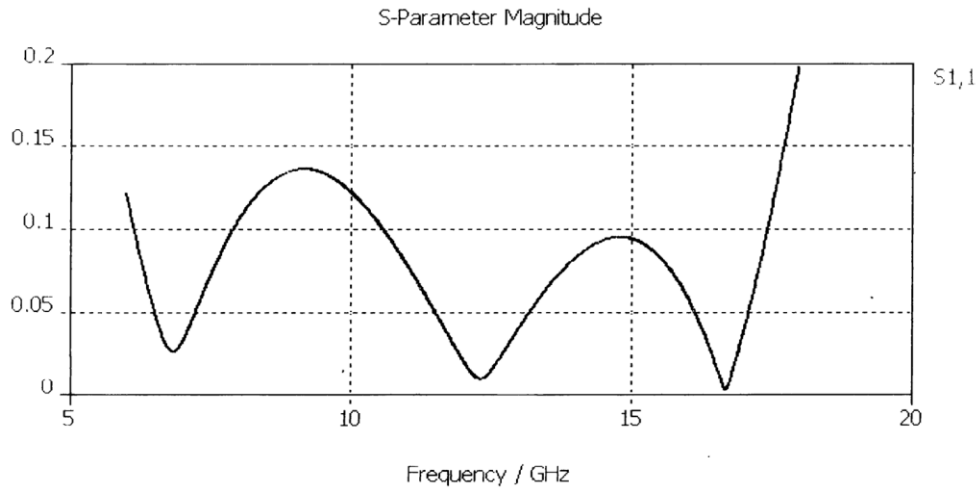


Fig. 5.1

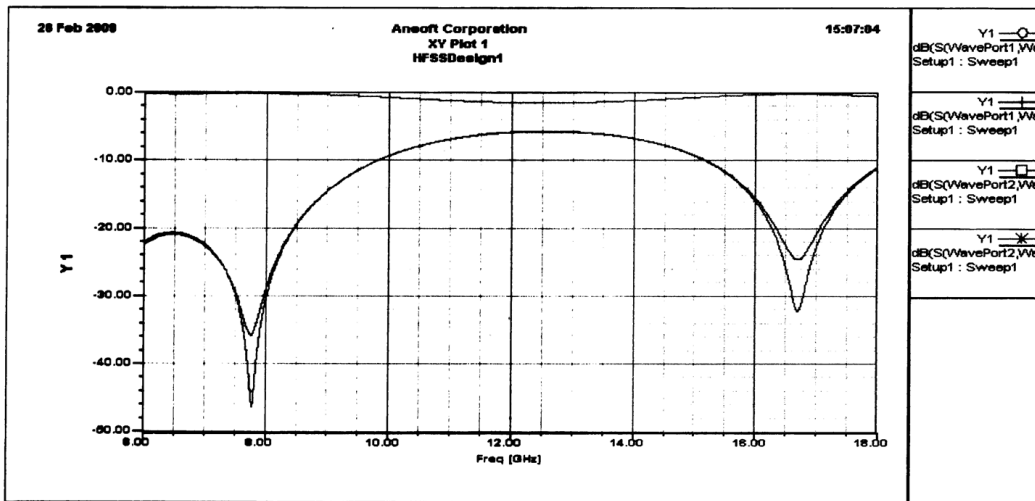


Fig. 5.2

The signal at the input port:

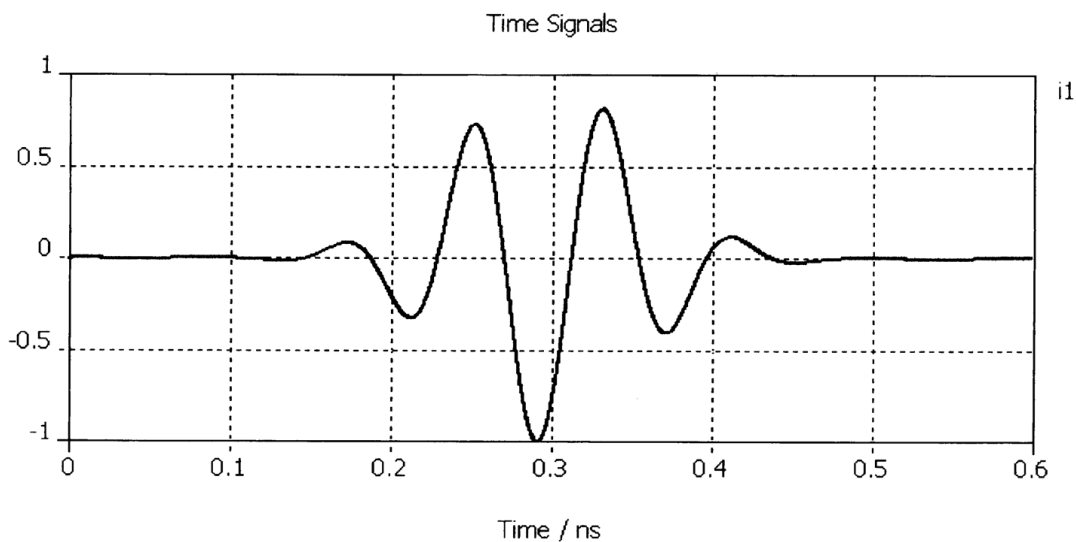


Fig. 5.3

The signals at the two output ports where the signals are reflected are O1, 1 and O2, 1

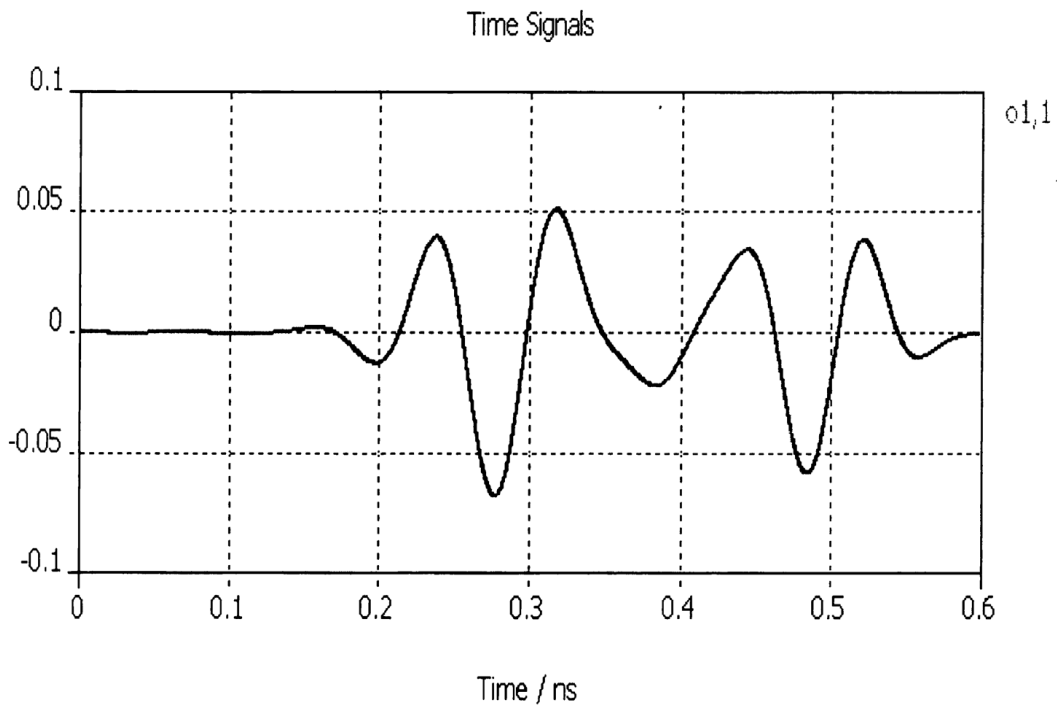
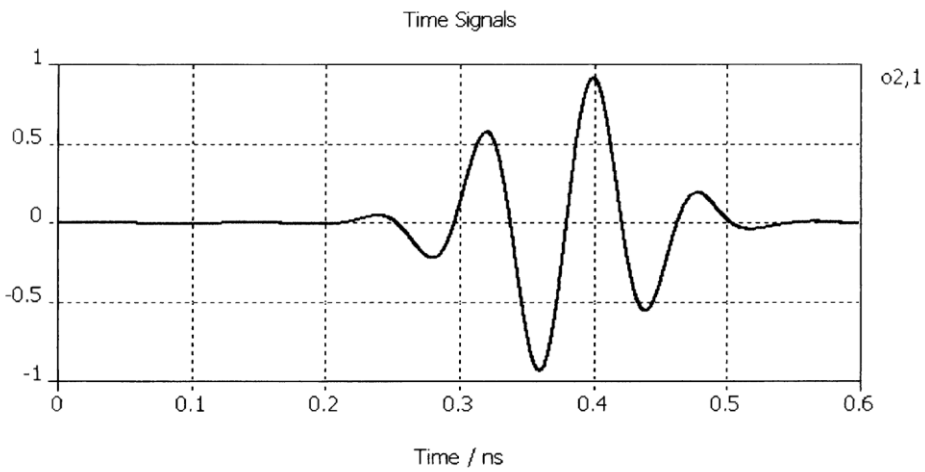
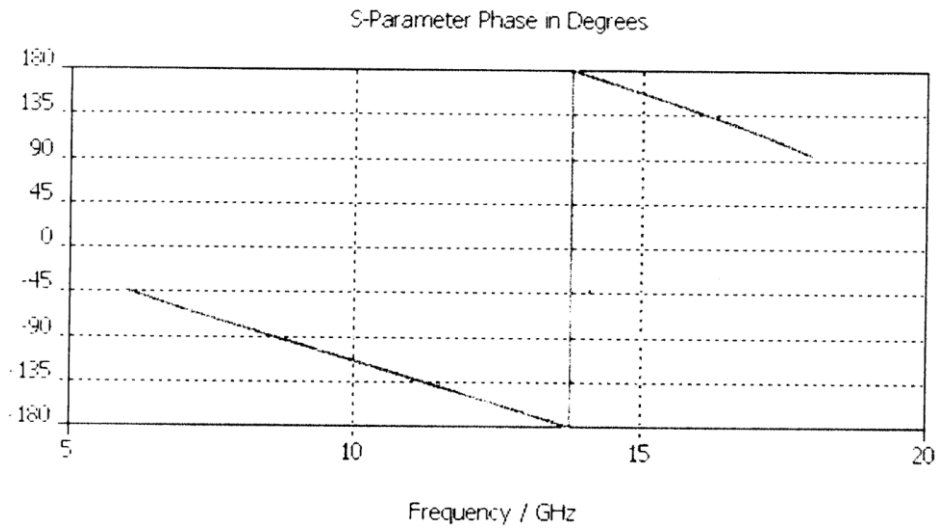


Fig. 5.4



**Fig. 5.5**

The s-parameter phase in degrees are given below :



**Fig. 5.6**

The Smith chart for S-Parameters in given below in CST software:

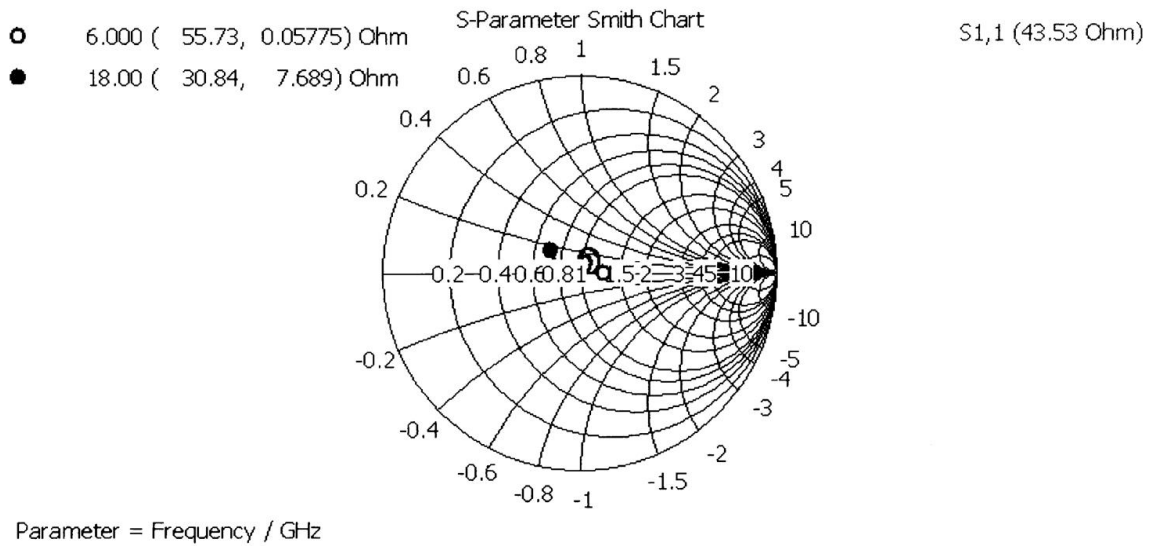


Fig. 5.7

The smith chart for S-parameters in HFSS is given below:

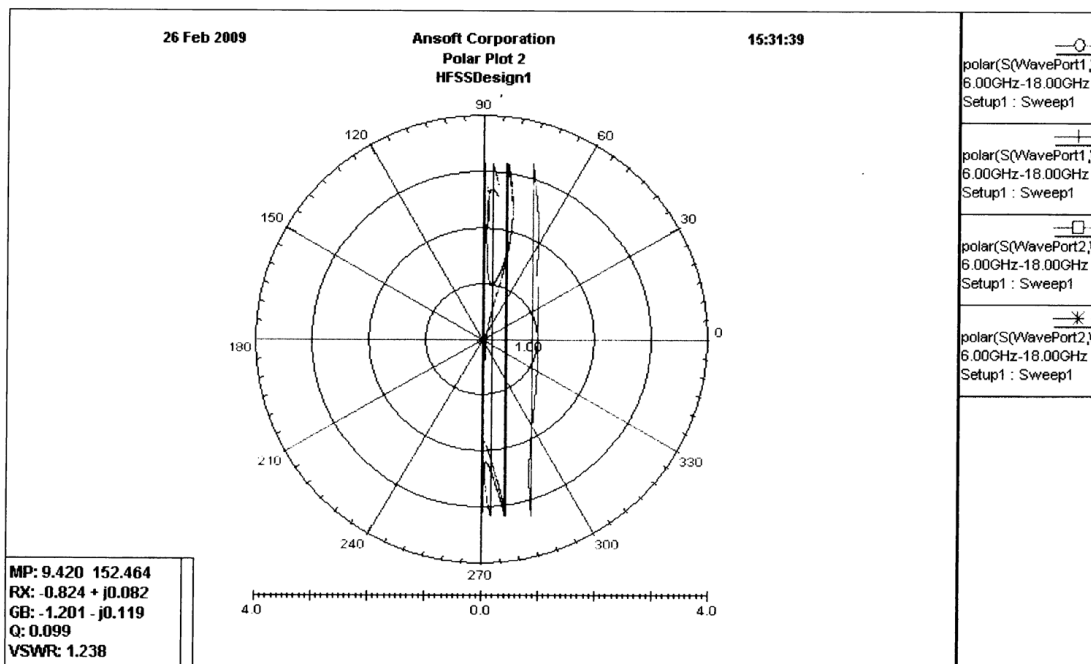


Fig. 5.8

The total field energy through time is given below:

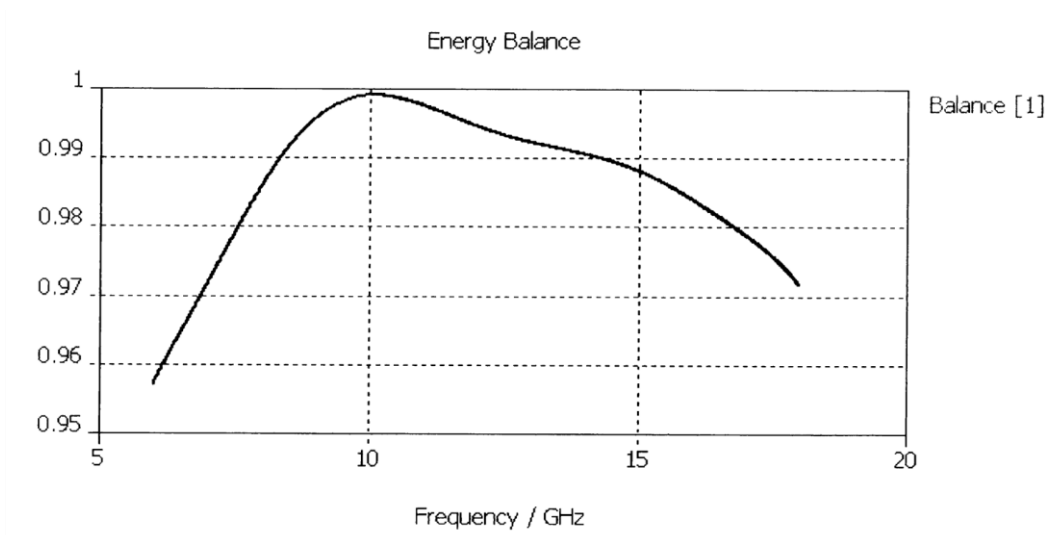


Fig. 5.9

The adaptive field energy /db is given below in CST:

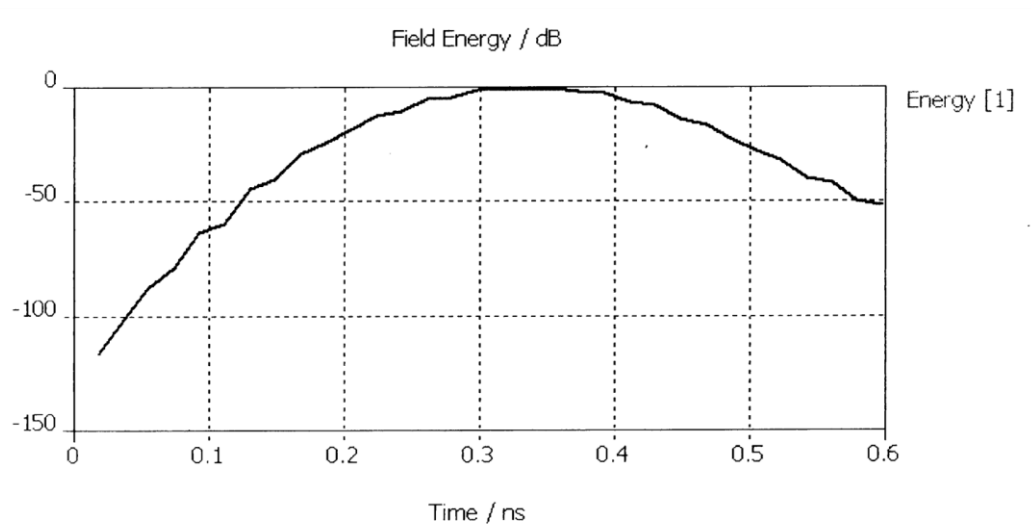


Fig. 5.10

The electric Field Distribution is given by:

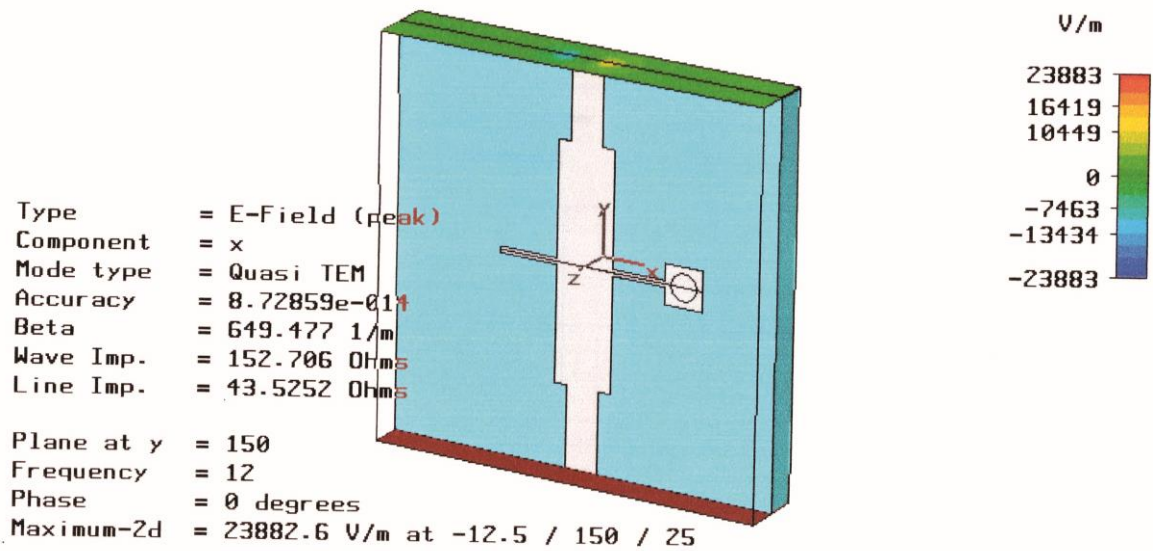


Fig. 5.11

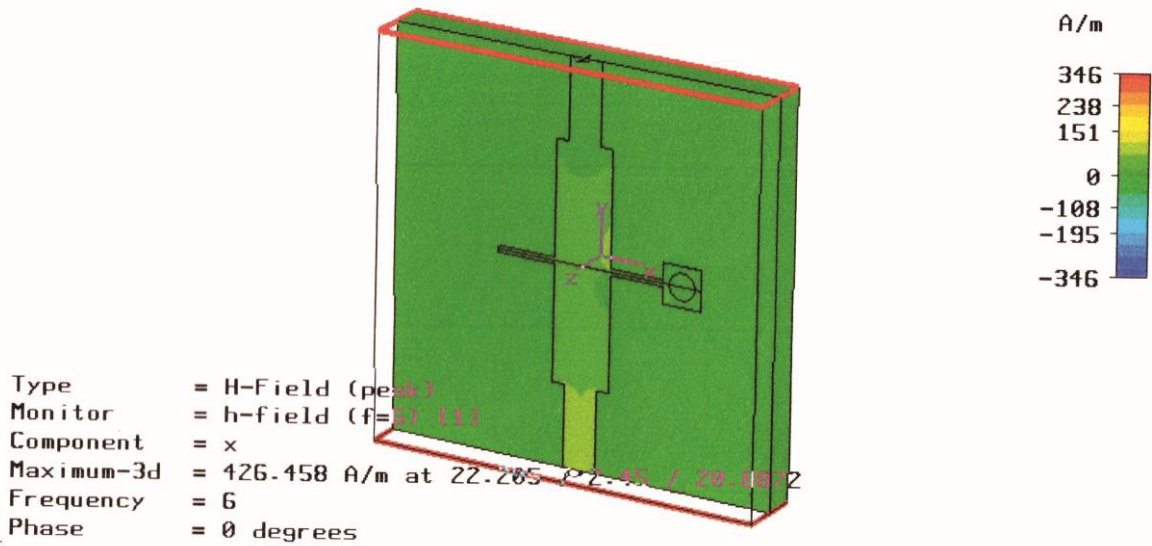


Fig. 5.12

Y-Parameters

$$I_1 = Y_{11} V_1 + Y_{12} V_2$$

$$I_2 = Y_{21} V_1 + Y_{22} V_2$$

The HFSS and CST results are as follows

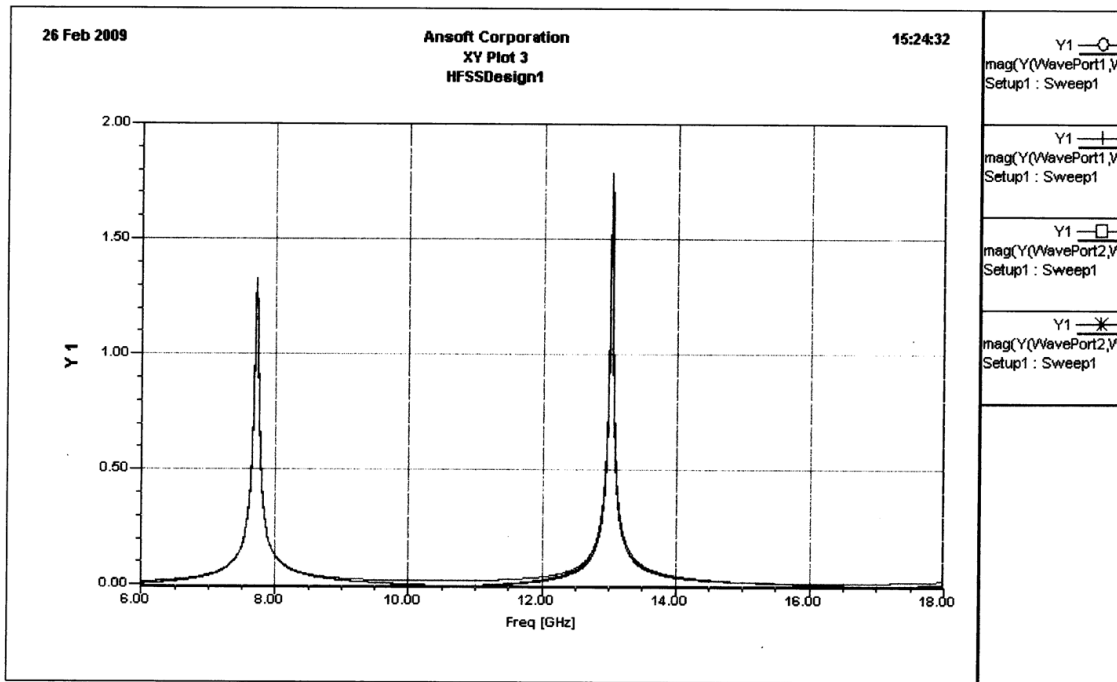


Fig. 5.13

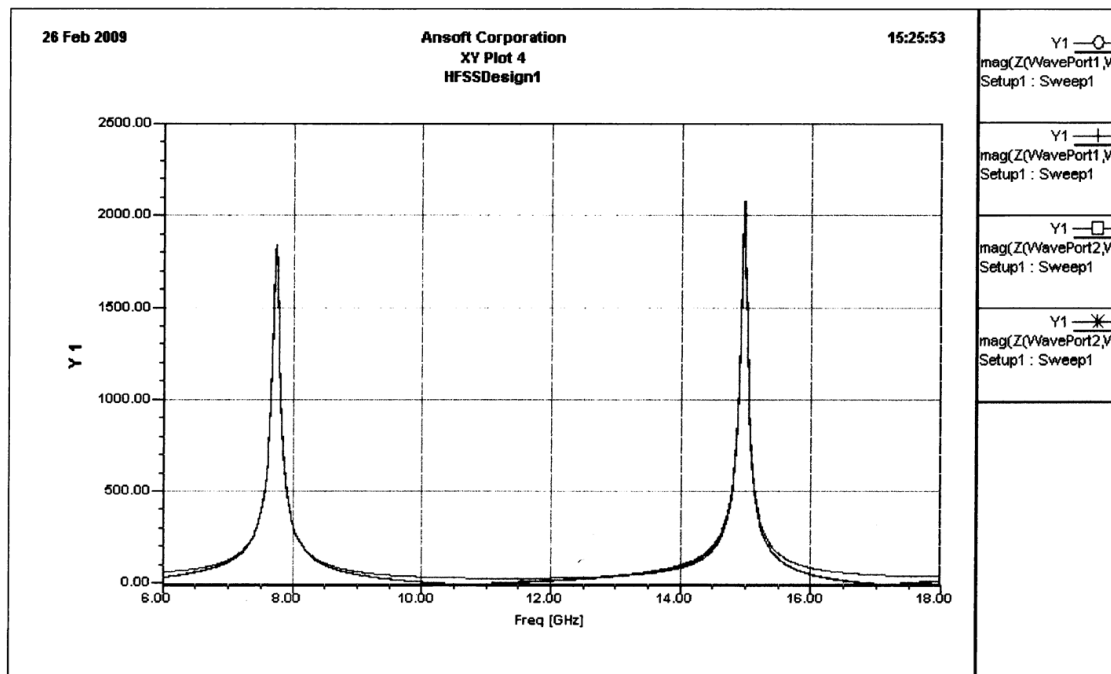


Fig. 5.14



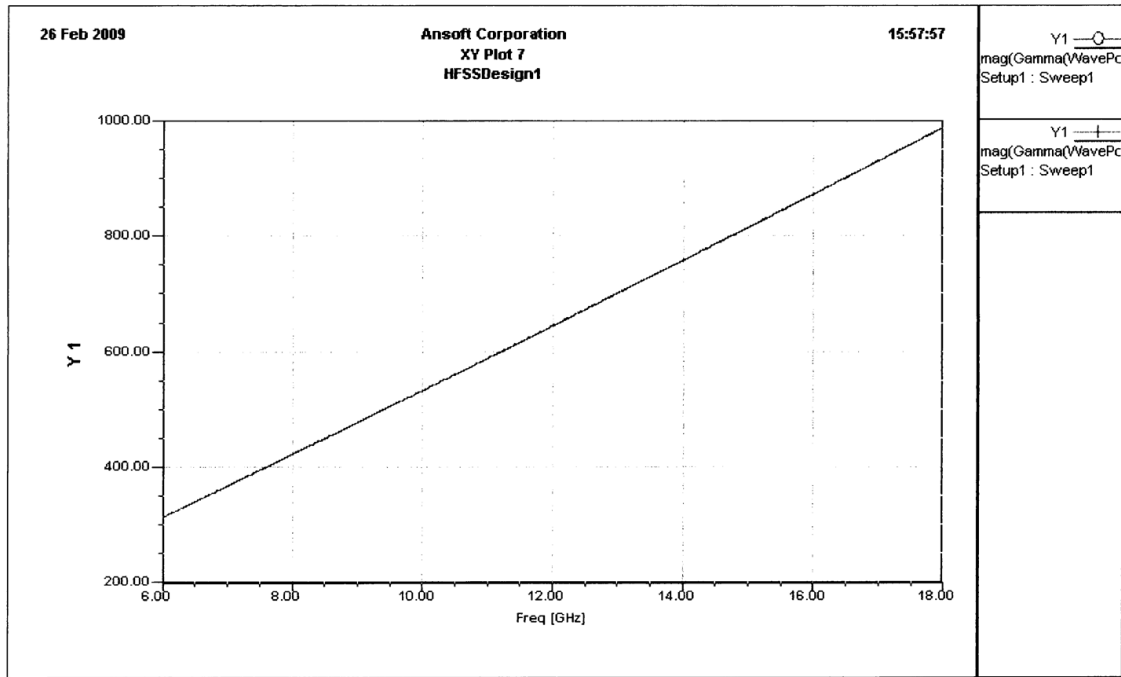


Fig. 5.15

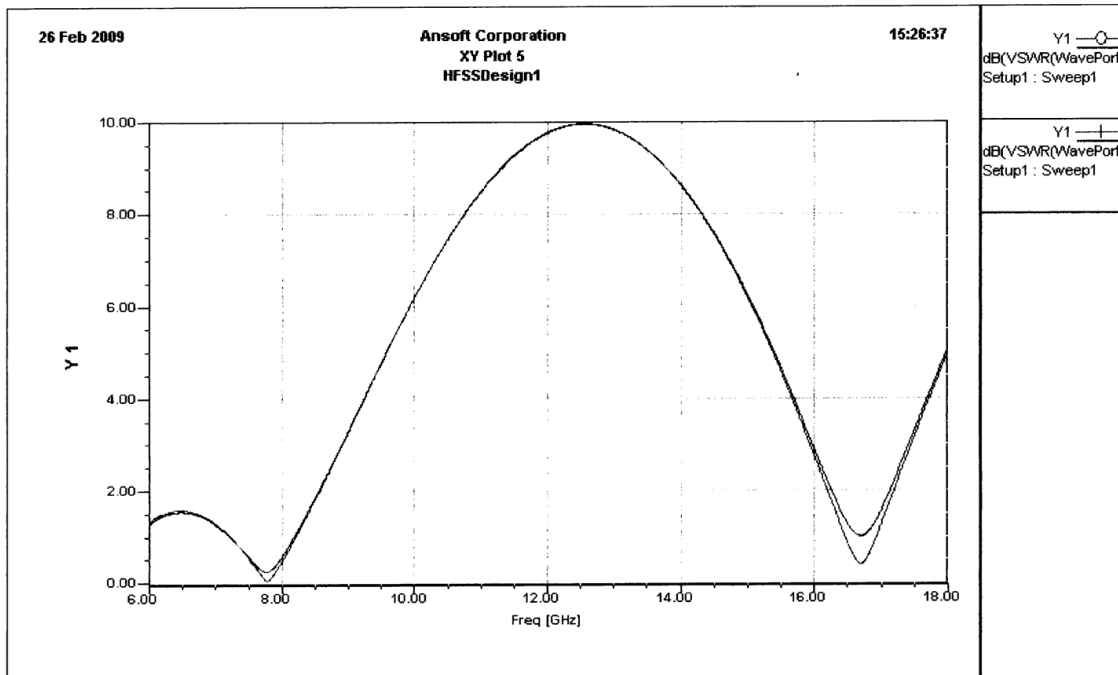


Fig. 5.16

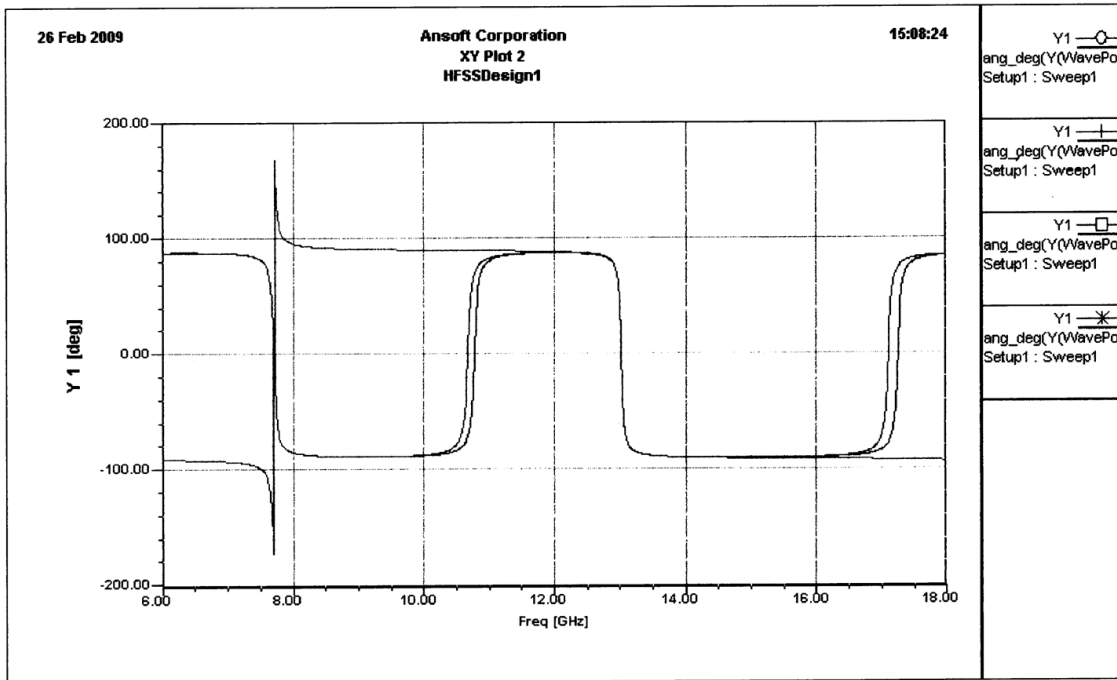


Fig. 5.17

**Characteristics impedance with variable d, w, h using FDTD program**

<b>d</b>	<b>w</b>	<b>h</b>	<b>Characterics Impedence (Zo)</b>
0.1	1	0.01	2.4073e+013
0.2	1	0.02	2.1793e+007
0.3	1	0.02	2.1793e+007
0.4	1	0.02	2.1793e+007
0.5	1	0.02	2.1793e+007
0.6	1	0.02	2.1793e+007
0.7	1	0.02	2.1793e+007
0.8	2	0.02	Inf
0.9	2	0.02	Inf
1.0	2	0.02	Inf

## CONCLUSION

The aim of the thesis work was to analyze the various characteristics of micro-strip phase shifter (micro-strip fitter), and to study their feed mechanism. It was also aimed to have a deeper understanding of the literature of the subject and to compare their results using two software's CST and HFSS. The aim was achieved to a reasonable degree.

In Chapter 2 an analysis of a simple micro-strip line is given which is used to find out relative  $\epsilon_r$ , characteristic impedance ( $Z_0$ ), loss tangent etc. These parameters could not be found out for the exact design because the PEC of the design was a variable one and it consists of two waveguide ports, the design also consists of a metallic cylinder which protrudes through the dielectric to the ground plane.

In Chapter 3 a brief discussion about the basic concepts and theory of fitter has been illustrated. This chapter also explains how a micro-strip phase shifter can act as a fitter.

In Chapter 4 & 5 the theory behind both CST and HFSS software are given and the results is simulated at a frequency range of 6-18 GHz. The results include the S-parameters, Y-parameters, VSWR circle, Switch chart, Characteristics impedance ( $Z_0$ ), the distribution of electric and magnetic field.

## REFERENCES

1. Microstrip Filter for RF/Microwave Application, Jia Shen G. Hong & M.A. Lancaster.
2. Microwave Engineering by David Pozar.
3. A Popoulis, The Fourier Integral and its Application, McGraw Hill, New York, 1962.
4. C. Toker, M. Saglam, M. Ozme, and N. Gunalp, "Branch-Line Coupler Using Unequal line Lengths", IEEE Trans. Microw. Theory Tech., vol. 49, no. 4, pp.718-721, Apr.2001.
5. D. Wu and F. Barnes, 'Doped  $Ba_xSr_{1-x}TiO_3$  Thin Films for Microwave Device Applications at Room Temperature', Integrated Ferroelectrics, vol. 22, no. 1-4, pp. 811-825, 1998.
6. Darlington, "Synthesis of reactance four poles which prescribed insertion loss characteristics", J. Math. Phys. 30, 257-353, Sept. 1939.
7. De Flaviis, M. Noro, G. Franceschetti, and N. G. Alexopoulos, "Application of Time domain Vector Potential Formulation to 3-D Electromagnetic Problems", in TSMMW '97 Topical Symposium on Millimeter Waves. Tokyo, Japan July 1997, pp.
8. E. Yamashita and K. Atsuki, "Stripline with rectangular outer conductor and there dielectric layers", IEEE Trans. Microwave Theory Tech., vol. MTT-18, May 1970.
9. F. De Flaviis, O.M. Stafsudd, and N. G. Alexopoulos, "Planer Microwave Integrated Phase Shifter Design with High Purity Ferroelectric Materials", IEEE Trans. Microwave Theory Tech., vol. 45, pp. 963-969, June 1997.
10. F. W. Van Keuls, R. R. Romanofsky, D. Y. Bohman, M. D. Winters, F. A. Miranda, C. H. Muller, R. E. Treece, T. V. Rivkin, and D. Galt,  
  
'(YBa<sub>2</sub>Cu<sub>3</sub>O<sub>7-δ</sub> Au) SrTiO<sub>3</sub>/LaAlO<sub>3</sub> thin film conductor/ferroelectric coupled microstripline phase shifters for phased array applications', Appl. Phys. Lett., vol. 71, no. 21, pp. 3075-3077, 1997.
11. G. C. Temes, and S. K. Mitra, Modern Fitter Theory and design, Wiley, New York, 1973.
12. G. M. Rebeiz, Guan-Leng Tan and J. S. Hayden, "RF MEMS phase shifters : design and applications", IEEE Microwave Magazine, vol.3, pp. 72-81, June 2002.

13. G. Mattaei, L. Young and E. M. T Jones, Microwave Fitters, Impedance Matching Network and Coupling Structures, Artech House Norwood, MA, 1980.
14. H. Ozaki and J. Ishill “Synthesis of a class of strip-line fitters”, IRE, Trans. Circuit theory, CT-5, 104109, June, 1958.
15. Haw-Jyh Liaw and H. Merkelo, “Signal integrity issues at split ground and power planes”, Electronic Components and Technology Conference, pp. 752-755, May 1996.
16. Hector J. De Los Santos, “Applications of MEMS Technology to RM/Microwave Systems”, ANTEM 2002 Symposium on Antenna Technology and Applied Electromagnetics, Montreal, Canada, pp.7-10, July-August 2002.
17. J. D. Rhoades, Theory of Electrical Fitters, Wiley, New York, 1976.
18. J. Helszajn, Synthesis of lumped element, Distributed and Planar Fitters McGraw Hill, London, 1990.
19. J. J. Green, E. Schlomann, F. Sandy, and J. Saunders, “Characterization of the microwave tensor permeability of partially magnetized materials”, R.A.D.C. TR 6963, Feb. 199, Rome Air Development Center, A.F.S.V.-G.A.F.B., NY.
20. J. S. Hayden and G. M. Rebeiz, “One and Two-Bit Low-Loss Cascadable MEMS Distributed X-Band Phase Shifters”, IEEE MIT-S Int. Microwave Symposium, Boston, USA, pp.161-164, 2000.
21. Jansen, “A modified least-squares boundary residual (I.S.B.R) method and its applications to the problem of shielded microstrip dispersion”, Arch. Elek. Ubertragung., Band 28, Heft 6, 1974.
22. Kondylis, G. Pottie, and F. De Flaviis, “Reduced FDTD Formulation (R-FDTD) for the solution of Maxwell Equations”, IEEE Microwave Letter, vol. submitted.
23. L. Wienberg, Network Analysis and Synthesis, McGraw Hill, New York, 1962.
24. P. I. Richards, “Resistor-transmission-line-circuits”, Proc. IRE, 36, 217-220, Feb, 1948.
25. R. Mitra and T. Itoh, “Analysis of microstrip transmission lines”, in Advances in Microwaves, vol. 8, New York : Academic Press, 1974.
26. R. Saal and e. Uibrich, “On the design of fitter by synthesis”, IRE Trans. CT-5, 284-327, Dec. 1958.

27. S. B. Cohn, "Dissipation loss in multi-coupled resonator fitter", Proc. IRE, 47, 1342-1348, August 1959.
28. S. S. Liao, P. T. Sun, N. C. Chin, and J. T. Peng, "A Novel Compact Size Branch-Line Coupler", IEEE Microw. Wireless Compon. Lett., vol. 15, no. 9, pp. 588-590, Sep. 2005.
29. T. Metzler, "Microstrip series Arrays", IEEE Trans. Antennas Propag., vol. AP 29, no. 1, pp. 174-178, Jan. 1981.
30. W. Cauer, Synthesis of Linear Communication Network, McGraw Hill, New York, 1958.
31. W. E. Thomson, "Delay Network having maximally flat frequency characteristics, Proc. IEE, 96- 487-490, Nov. 1949.